EGR2 promoter antisense RNA coordinates chromatin remodeling and spatial genome organization in Schwann cells.

Margot Martinez-Moreno[1], David Karambizi[1*], Hyeyeon Hwang[1*], Kristen Fregoso[1], Jia-Shu Chen[1], Eduardo Fajardo[2], Andras Fiser[2], Nikos Tapinos[1,3,4]

1: Laboratory of Cancer Epigenetics and Plasticity, Brown University, Providence, RI, USA

2: Department of Systems and Computational Biology, Albert Einstein College of Medicine, Bronx, NY, USA

3: Department of Neurosurgery, Brown University, Rhode Island Hospital, Providence, RI, USA

4: Cancer Biology Program, Brown University, Lifespan Cancer Institute, Providence RI, USA

***: These authors contributed equally to the work**

¶: Corresponding Author:

Nikos Tapinos M.D., Ph.D.

Laboratory of Cancer Epigenetics and Plasticity

Brown University

e-mail: nikos_tapinos@brown.edu

Highlights

- Overexpression of the *EGR2*-AS-RNA regulates gene expression in Schwann Cells
- The *EGR2*-AS-RNA binds and recruits repressive and activating chromatin modifiers on the *EGR2* and *C-JUN* promoters, repsectively
- ATAC-seq data showed an increase in the AP-1 network accessibility/TF activity
- The *EGR2*-AS-RNA promotes reorganization of the global chromatin landscape, quantitative changes in loop formation and in contact frequency at domain boundaries exhibiting enrichment for AP-1 genes

Summary

The *EGR2* promoter antisense RNA (AS-RNA) recruits chromatin remodeling complexes to inhibit *EGR2* transcription following peripheral nerve injury. Here we show that the *EGR2*-AS-RNA modulates chromatin accessibility and serves as scaffold for two distinct histone modification complexes. It binds to EZH2 and WDR5 and enables coordinate targeting of H3K27me3 and H3K4me3 to promoters of *EGR2*and *C-JUN*. Expression of the AS-RNA results in reorganization of the global chromatin landscape and quantitative changes in loop formation and in contact frequency at domain boundaries exhibiting enrichment for AP-1 genes. In addition, the *EGR2*-AS-RNA induces changes in hierarchical TADs and increases transcriptional activity on an inter-TAD loop between a super-enhancer regulatory hub and the promoter of *mTOR*. Our results show that the *EGR2*-AS-RNA may serve as regulator of coordinate chromatin remodeling and spatial genome organization to regulate cellular plasticity-associated transcription in Schwann cells.

Keywords

Antisense-RNA, *EGR2*, *C-JUN*, EZH2, WDR5, H3K27me3, H3K4me3, AP-1, *mTOR*

Introduction

Spatial genome organization involves the three-dimensional (3D) structure, positioning, and interactions of chromatin within the nucleus. This is a non-random process and is prone to regulation within various nuclear domains, topological associations and through chromatin modifying epigenetic mechanisms. In recent years, non-coding RNAs (ncRNAs) have emerged as major regulators of spatial genome organization. ncRNAs are RNA molecules that are not translated into proteins and are implicated in numerous cellular processes including transcription, mRNA splicing, and protein translation (Khalil et al., 2009; Mortazavi et al., 2008; Palazzo and Lee, 2015). ncRNAs impact spatial genome organization by modulating perinuclear chromosome tethering, the formation of major nuclear compartments, chromatin looping and various chromosomal structures (Khosraviani et al., 2019). These roles of ncRNAs often intersect with various other protein or nucleic acid components of genome structure and function. Although the role of ncRNAs as modulators of the 3D genome organization of the X Chromosome, various developmental genes and repetitive DNA loci (Khosraviani *et al.*, 2019) has been described, the exact mechanistic role of the low-copy promoter associated antisense RNAs (AS-RNAs) in gene regulation, chromatin remodeling and spatial genome organization is not known.

The peripheral nervous system (PNS) exhibits a unique ability of tissue regeneration, mainly due to the remarkable plasticity of Schwann cells (SCs). Following nerve lesion, SCs reprogram into proliferative progenitor-like repair SCs, that drive the regenerative process, involving down-regulation of pro-myelinating/differentiation genes (e.g. *EGR2*/*KROX20, MPZ* and *MBP*) and up-regulation of genes that define repair SCs (including *C-JUN* and *GDNF*) (Figlia, 2018). There are

many transcription factors involved in SC plasticity and regeneration after injury (Jacob, 2015; 2017; Jessen and Mirsky, 2019a; b; Sock and Wegner, 2019; Stierli et al., 2019; Svaren and Meijer, 2008). Among those, SOX10, OCT6, and EGR2/KROX20 have major functions in the myelination and remyelination processes (Weider and Wegner, 2017). SOX10 and OCT6 together activate the expression of EGR2, which in turn activates the expression of myelin genes together with SOX10 and is thus essential for myelination (Ghislain et al., 2002; Kuhlbrodt et al., 1998; Topilko et al., 1994). After injury, a different set of transcription factors controls SC demyelination and conversion into repair cells (Jessen and Arthur-Farraj, 2019). Among those, C-JUN is a master inducer of the switch to the repair phenotype (Arthur-Farraj et al., 2012; Gomez-Sanchez et al., 2015). Collectively, molecular mechanisms that influence the balance of transcriptional activity between EGR2 and C-JUN are critical in the process of SC plasticity and nerve regeneration.

We have previously mapped a promoter antisense RNA complementary to the *EGR2* promoter in Schwann cells (*EGR2*-AS-RNA), showed that its expression is increased following peripheral nerve injury and that it mediates the recruitment of EZH2 and H3K27me3 on *EGR2* promoter to induce transcriptional silencing of *EGR2* (Martinez-Moreno *et al.,* 2017). Here we reveal the mechanistic function of this promoter AS-RNA and show that it works as a molecular scaffold to bring together WDR5, EZH2 together with activating (H3K4me3) and repressing (H3K27me3) histone marks on the promoters of *C-JUN* and *EGR2* respectively. Expression of the *EGR2*-AS-RNA induces chromatin remodeling and increased chromatin accessibility in promoters of genes encoding the AP1 transcription factor family. Finally, interrogation of 3D genome architecture using Hi-C reveals that expression of the *EGR2*-AS-RNA in SCs induces re-organization of the 3D architecture of the SC genome, quantitative changes in hierarchical topologically associating domains (TADs) and increased transcriptional regulation on an inter-TAD interaction between a

super-enhancer like regulatory hub and the promoter of *mTOR*. We propose a new model for promoter AS-RNA-mediated transcriptional regulation orchestrated by the molecular scaffold activity of the AS-RNAs that recruit chromatin modulators to reorganize chromatin and 3D genome architecture in hubs that define cellular plasticity.

Results

Expression of the *EGR2*-AS-RNA results in transcriptomic changes in Schwann Cells

To determine the effect of the *EGR2*-AS-RNA on global gene expression we infected Schwann cells (SCs) with a lentivirus expressing the AS-RNA (Lenti-AS) as previously described (Martinez-Moreno *et al.*, 2017). First, we assessed transcript levels of the AS-RNA following its overexpression and noted an average of 2,223 reads on the *EGR2* promoter site. This is in comparison to the GFP control samples (Lenti-GFP), which showed 242 reads on average suggesting low baseline expression (Figure 1A). Next, we conducted gene expression analysis on the RNA-seq data in order to probe global gene expression changes. We noted 561 differentially expressed genes. 111 were downregulated and 450 upregulated (Figure 1B). Principal component analysis (PCA) between RNA-seq biological replicates from Lenti-GFP and Lenti-AS SCs showed that the replicates clustered together, and the results were highly reproducible (Figure S1A). Upregulated genes were enriched for mTOR signaling, Sonic Hedgehog (SHH) signaling and cell cycling biological processes. Downregulated genes were enriched for ERK1/ERK2 signaling, ERbB signaling pathways, MAPK regulation and ECM organization biological processes (Figure 1C).

The *EGR2*-AS-RNA inhibits EGR2 and activates C-JUN expression in SCs

We have shown that overexpression of the *EGR2*-AS-RNA results in demyelination, while inhibition of the *EGR2*-AS-RNA expression in vivo delays the dedifferentiation of myelinating

SCs (Martinez-Moreno *et al.*, 2017). Since EGR2 and C-JUN transcription factors control the balance of differentiation and dedifferentiation of SCs (Arthur-Farraj *et al.*, 2012), we examined if overexpression of the *EGR2*-AS-RNA has opposing effects on the expression of EGR2 and C-JUN. We infected SCs with Lenti-AS or Lenti-GFP and show that ectopic expression of the *EGR2*-AS-RNA inhibits the expression of EGR2 protein and induces the expression of C-JUN (Figure 1D). In order to out rule that the increase of expression of C-JUN is due to the direct inhibition of EGR2 by the AS-RNA, we inhibited EGR2 expression in SCs using siRNAs (Figures S1C) and show that *C-JUN* transcript expression is significantly downregulated following EGR2 inhibition by siRNAs in SCs (Figure S1D). Taken together, our results suggest that the *EGR2*-AS-RNA could regulate *C-JUN* in *trans* through a different molecular mechanism that does not depend on the direct inhibition of EGR2.

The *EGR2*-AS-RNA acts as molecular scaffold for EZH2 and WDR5 to enable coordinate targeting of H3K27me3 and H3K4me3 at *EGR2* and *C-JUN* promoters

We have shown that the *EGR2*-AS-RNA has a direct repressive effect on the *EGR2* promoter after sciatic nerve injury by recruiting components of the Polycomb Repressive Complex (PRC) (Martinez-Moreno *et al.*, 2017). The repair SC phenotype is characterized by the activation of certain factors, such as C-JUN, and histone modifications are key to the regulation of these genes after injury (Duman et al., 2020). In order to determine whether the regulation of *EGR2* and *C-JUN* is mediated by the *EGR2*-AS-RNA in conjunction with chromatin modifying enzymes (CMEs) and histone marks, we performed RNA immunoprecipitation (RIP) and chromatin immunoprecipitation (ChIP) in SCs after overexpression of the *EGR2*-AS-RNA. We performed RIPs with antibodies against EZH2 and WDR5, and ChIPs with antibodies against the tri-methylated histone 27 (H3K27me3, repressive) and the tri-methylated histone 4 (H3K4me3,

activating) marks followed by qPCR to detect either the presence of the AS-RNA following RIP, or the presence of *EGR2* and *C-JUN* promoters binding to the histone marks (ChIP). The RIP experiment shows that both EZH2 and WDR5 pull down the *EGR2*-AS-RNA compared to the control samples (Figure 2A, left panels). In addition, overexpression of the *EGR2*-AS-RNA in SCs results in significant increase of H3K27me3 binding to the *EGR2* promoter, and significant increase in association of H3K4me3 to the *C-JUN* promoter (Figure 2A, right panels). This interaction was reverted with the addition of specific inhibitory oligonucleotide GapMers that target the AS-RNA, which suggests that the interaction of H3K27me3 and H3K4me3 with *EGR2* and *C-JUN* respectively depends on the presence of the AS-RNA (Figure 2A, right panels).

To verify that the AS-RNA functions as a scaffold to recruit both repressing (EZH2) and activating (WDR5) CMEs and the two proteins (EZH2 and WDR5) do not interact with each other in the absence of the AS-RNA, we performed co-immunoprecipitation (IP) experiments of WDR5 and EZH2 following overexpression of WDR5 in SCs. IP of FLAG-tagged WDR5 from SCs specifically retrieved WDR5 but not EZH2 (Figure 2B and Figure S2A) suggesting the two proteins do not form protein-protein interactions. Next, we determined if EZH2 and WDR5 interact with separate regions of the AS-RNA, which would suggest sequence-specific interaction as shown before for the lncRNA HOTAIR (Tsai et al., 2010). We cloned two equal-sized fragments of the AS-RNA corresponding to nucleotides -966 to -483 (AS1) and -482 to -1 (AS2) of the full length *EGR2*-AS-RNA sequence (Figure S2B and S2C). Overexpression of AS1 and AS2 in SCs (Figure S2D and S2E) followed by RIPs for EZH2 and WDR5 shows that EZH2 binds to the AS1 fragment, while WDR5 to the AS2 confirming region specific interactions (Figure 2C). These results suggest that the *EGR2*-AS-RNA is a bimodal AS-RNA that has distinct binding domains for EZH2 and WDR5 to recruit repressive (H3K27me3) and activating (H3K4me3) histone marks

on the promoters of *EGR2* and *C-JUN* (schematic at Figure 2D). To verify that expression of the AS-RNA has functional effects on promoter activity, we performed transcription factor (TF) activity assays following overexpression of the *EGR2*-AS-RNA to determine the activation of the transcription factor activity of C-JUN on the AP-1 specific binding motif. We show that the AS-RNA significantly increases TF activity of C-JUN (Figure 2E). The increase of C-JUN transcriptional activity is not secondary to the effect of the AS-RNA on EGR2 since we are unable to replicate this finding when we treat SCs with EGR2 specific siRNAs (Figure S2F).

The *EGR2*-AS-RNA induces chromatin remodeling and increased transcriptional activity of the AP-1/JUN family of TFs

We performed ATAC-seq to capture genome wide epigenetic profile changes induced by the AS-RNA transcript. First, we performed a PCA analysis, which showed that control and treated samples closely cluster together (Figure 3A, Figure 3SA) suggesting that the epigenetic changes induced by the AS-RNA are reproducible. We then performed a differential accessibility analysis and observed that the AS-RNA increased accessibility at 109 and decreased it at 467 sites (Figure 3B). Genes with increased accessibility showed significant enrichment for the AP-1 transcription factor network (Figure 3C). Promoter of genes such as *JUN*, *JUNB*, *JUND*, *FOSB*, *FOS* saw a significant increase in accessibility following AS-RNA overexpression (Figure 3D, Figure S3B). Next, using accessibility data, we performed transcription factor (TF) footprinting analysis to interrogate TF activity. We found that the AP-1 TF family and the architectural protein CTCF (CTCF zinc finger family) experience the most significant increase in TF activity following AS-RNA expression (Figure 3E, Figure 3F).

Expression of the *EGR2*-AS-RNA results in genome reorganization and a gain in stable loops associated with genes enriched for AP-1 TF network and NOTCH 1 signaling

We showed that the *EGR2*-AS-RNA functions as molecular scaffold to interact with chromatin modifiers that specify active and inactive chromatin states (Figure 2A, Figure 2D). In addition, ATAC-seq data showed that expression of the AS-RNA results in changes of CTCF activity (Figure 3F). Consequently, we hypothesized that ectopic expression of the AS-RNA may induce spatial genome reorganization in SCs. We performed Hi-C following expression of the AS-RNA using Lenti-AS and compared the genome architecture with SCs expressing Lenti-GFP as control (Figure S4). We identified stable loops structures defining contact points between genomic loci pairs (loop anchors) from the contact frequency map (Hi-C map) (Figure S5C). Overexpression of the AS-RNA resulted in a decrease in total loops (Figure S5A). Lenti-GFP samples had an average detection of 86,382 significant interactions (loops), while Lenti-AS samples had 68,901 loops on average (Figure S5A). Loops in the AS-RNA samples made shorter range interactions compared to control samples (Figure S5B). Next, we performed differential loop analysis to identify changes in putative loop interactions that are due to the AS-RNA overexpression. These were labelled as static, gained and lost loops according to changes in interaction frequency. Though most loops/interacting loci were static, we found 545 loops that changed following AS-RNA overexpression (Figure 4A). 104 loops were gained and 441 lost (Figure 4A). The dynamic loops made shorter range interactions than static loops (Figure 4B). Overall, most loops lost interactions, and this was consistent across all chromosomes (Figure S5D).

Putative, stable loops generally represent sites of regulation and may facilitate cis-regulatory element to cis-regulatory element, promoter to promoter or cis-regulatory element to promoter interactions. We proceeded to annotate gene promoters existing at the loop anchors (Figure 4C). This allowed us to further characterize the loops. We found that promoters annotated to the gained loops were enriched for the AP-1 TF network and NOTCH1 signaling (Figure 4D). Lost loops

were enriched for C-MYC signaling, β-CATENIN and SMAD2/3 signaling (Figure 4D). Finally, static loops were found to be enriched for ERBB signaling and mTOR signaling (Figure 4D).

Integrated 3D genome reconstruction reveals clusters of cis-regulatory elements (CORES) and associated promoters in Schwann cells

We sought to integrate gene expression analysis, chromatin accessibility data, TF footprinting and genome interaction frequency to reconstruct a comprehensive 3D genome organization of SCs in response to *EGR2*-AS-RNA expression. Hi-C defines loops that are 1) either structural in nature or 2) function to bring together DNA regulatory elements. To identify the latter, we found loops whose contact point (anchors) involves a promoter and its regulatory element (Figure 5A). Previous work has shown that DNA regulatory regions such as promoters, enhancers, silencers and insulators are in open chromatin, nucleosome depleted areas (Cockerill, 2011). A limited set of such accessible sites are composed of large intergenic clusters of accessible chromatin sites (<20 Kb apart) that are cell type specific, hence reminiscent of super enhancers (Gaulton et al., 2010; Madani Tonekaboni et al., 2019; Song et al., 2011). These regions were dubbed "clusters of cis-regulatory elements" or COREs. Using an unsupervised machine learning approach, we identified an average of 309 and 472 of such clusters (CORES) in control and AS-RNA samples, respectively (Figure S6A). Additionally, we noted a heavy TF occupancy at 40% of the COREs with a median occupancy of 155 footprints (Figure 5B, Figure S6C). These data cast half of the COREs as being highly active regulatory DNA sites.

Distal DNA regulatory elements with significant TF occupancy are known to form regulatory, stable loops at promoters. To identify these loop structures, we identified loops whose anchors join a distal CORE and its target promoter(s) (Figure 5A). Approximately 10% (157/1563 total CORES across all samples) contacted at least one promoter site (Figure 5C, Figure 5D). There were in total

192 unique long-distance genomic interactions between CORES and promoters (Figure 5C). These interactions occurred at median genomic distances of 365 Kb and 340 Kb in Lenti-GFP and Lenti-AS respectively (Figure S6B). Pathway enrichment analysis of the CORES interacting genes showed top enrichment for translation, mTOR signaling, protein metabolism, PI3KC1/AKT signaling and AMPK signaling (Figure 5E). Of the 192 genes whose promoter formed long range interactions with COREs, 15% of the genes (28/192) experienced a change in gene expression following AS-RNA overexpression (Figure 5F).

Expression of the *EGR2*-AS-RNA results in regulatory changes between the *mTOR* promoter and its cis-regulatory elements

Of the 192 COREs-promoter interactions, we focused on regulation at the *mTOR* promoter. Beyond its established (Beirowski et al., 2017) significance in SC plasticity, we elected to further probe regulation at this promoter for the following reasons: 1) *mTOR* belonged to the 28 CORES-promoter interactions that resulted in changes in gene expression following AS-RNA overexpression (Figure 5E); 2) this interaction was reproducible across samples (Figure 6A); 3) *mTOR* promoter interacts with a large cluster of regulatory elements (a region covering ~100 Kb) reminiscent of a super enhancer (Figure 6A); and 4) the *mTOR* region was one of few regions forming multiple contacts with a CORE (8 interactions total), potentially suggesting a regulatory hub (Figure 8A). We tested whether this regulatory region uniquely interacts with the *mTOR* region by screening for all other possible interactions and found none. This suggests that we discovered an *mTOR* regulating super enhancer/regulatory region located ~336 Kb bases away from the *mTOR* promoter (Figure 6A).

Lower resolution inspection of contact frequencies at the COREs-*mTOR* locus (500 Kb-~1 Mb resolution) revealed that *mTOR* and its regulating super enhancer region are in different domains

(Figure S7A, Figure S7C). Closer inspection of COREs-*mTOR* promoter interaction showed three main points of contact that originate from the COREs region and perfectly contact the *mTOR* promoter (Figure S7A, Figure 6A). We further differentiate these contact points based on distance from the nearest TAD boundary, labelled "nearest distance", "mid distance" and "farthest distance" to TAD boundary (Figure 6A, Figure S7B). These contact points harbored significant TF activity with 408 footprints on aggregate (Figure S7B). We noted increasing TF occupancy as the contact sites approached the TAD boundary (Figure S7B). Next, we clustered the TFs present at the "nearest distance", "mid distance" and "farthest distance" to TAD boundary in TF communities based on the presence of families of TFs. The farthest distance to boundary interaction showed only REST occupancy, a well-known repressive transcription factor in neuronal lineage cells (Figure 7C, Figure S7B). The mid distance to TAD boundary had 65 TFs with an enrichment for the C2H2 zinc finger class of TFs, such as GLI3, GLI2, GLIS3, GLIS2 and MAZ (Figure 7B, Figure S7B). The nearest to TAD contact had 342 TF with a predominance for the AP-1 family of TFs, structural TFs such as CTCF, VEZF1 and MAZ and for zinc fingers of the Kruppel family (Figure 7A, Figure S7B). Finally, we found an increase in TF activity of the AP-1 family, FOX family, Tryptophan cluster class, TEA domain class, RHR class and GLI family after AS-RNA overexpression (Figure 6C).

The *EGR2*-AS-RNA induces changes at the *mTOR* interdomain regulatory hub

We determined that the COREs-*mTOR* interactions occur via an interdomain contact (Figure S8A, Figure S7A, Figure 8A, Figure S7C). While most of all interactions occur within TADs, 30% of interactions occur between TADs (Figure S8D). Additionally, we found that these interdomain interactions occurred mostly in non-adjacent TADs (Figure S8D). The *mTOR* and COREs harboring TADs, which both occupy active compartments (A compartments), exhibit preferential

interdomain interactions (Figure S8A, Figure S8B). We detected 8 total interactions linking the CORE containing TAD and the *mTOR* containing TAD (Figure 8A). This was one of the highest noted interactions between a CORE and a gene region. Additionally, we noted >400 footprints at *mTOR* promoter contacting COREs, far superseding the median occupancy of 155 footprints found at all COREs across all samples (Figure S7B, Figure S6C). The stability of the interactions and the high TF occupancy suggested a heavily regulated hub between the *mTOR* promoter and its interacting super-enhancer region.

Next, we probed changes occurring at this *mTOR* regulatory hub following AS-RNA overexpression. We observed both TF activity and structural changes at the hub. First, there was an overall increase in TF activity at the hub following AS-RNA overexpression, with notable increase in binding scores of the AP-1 TF family and FOX TF family (Figure 6B, Figure 6C, Figure 7A, 7B, 7C, Figure 8B). Second, we noted the formation of a new boundary at the 3' end of the *mTOR* gene after AS-RNA overexpression (Figure 8C). This new boundary resulted in the formation of a nested sub structure, whereby *mTOR* is more insulated from other possible intra and inter TAD interactions (Figure 8C). Such changes may function to maximize *mTOR*-CORE interaction, while minimizing other interactions. The TF activity and structural changes at the *mTOR* interaction hub were accompanied with moderate, but statistically significant increase in *mTOR* expression levels following AS-RNA overexpression (Figure 8D, Figure 8C, Figure S8C).

Discussion

Recently, we demonstrated that an *EGR2* promoter antisense RNA is induced following in vivo sciatic nerve injury. The AS-RNA inhibits *EGR2* transcription via recruitment of components of the PRC2 complex (EZH2, H3K27me3) to the *EGR2* promoter, while inhibition of the AS-RNA expression delays demyelination in a sciatic nerve transection model (Martinez-Moreno *et al.*,

2017). It has been shown that long non-coding RNAs can have opposing regulatory effects by simultaneously binding to epigenetic activators and inhibitors (Akhade et al., 2017; Rinn and Chang, 2012) but this role has not been established for promoter antisense RNAs. We show here that the *EGR2*-AS-RNA functions as a molecular scaffold that recruits activating and repressing histone marks on the promoters of *C-JUN* and *EGR2* respectively. RNA immunoprecipitation confirmed that the *EGR2*-AS-RNA binds to both EZH2 and WDR5 in a sequence-specific manner. EZH2 is a methyltransferase that activates the repressive histone mark H3K27me3, while WDR5 is required for binding of the methyltransferase complex to the activating histone mark H3K4me3. Both EZH2 and WDR5 have been described to be cofactors of their own complexes (PRC2 and MLL complexes). Our data show that EZH2 and WDR5 do not precipitate together and do not bind to the same region of the AS-RNA, suggesting that the AS-RNA has an instructive role in the recruitment of histone modifying enzymes with opposing functions. Next, we show that this AS-RNA scaffolding of CMEs results in downstream chromatin and architectural changes at plasticity and cell identity defining sites.

Recently it was shown that subtle changes in chromatin loop contact can lead to significant changes in gene expression (Greenwald et al., 2019). These loops can bring together the regulatory elements with their target sequences that can be distant from one another. After the AS-RNA overexpression, we observe a decrease in the total number of loops formed, and these loops make shorter range interactions relative to control samples. It has been suggested that larger loops may have a structural role, and could therefore be involved in the formation of insulated neighborhoods to protect and stabilize interactions between promoters and regulatory elements, while shorter range interaction loops may be more regulatory (Dowen et al., 2014; Ong and Corces, 2014; Phanstiel et al., 2017). In addition, our Hi-C data show enrichment of genes involved in AP-1 and

NOTCH1 signaling at the gained loop anchors suggesting that AP-1 and NOTCH1 signaling network experience a change in regulation due to increased contact with distal regulatory elements following expression of the AS-RNA. AP-1 is a heterodimeric TF consisting of combinations of FOS, JUN, MAF, ATF and CREB. The AP-1 family member C-JUN is a master regulator involved in SC reprogramming and its expression is highly induced after nerve injury and during peripheral neuropathies (Arthur-Farraj *et al.*, 2012; Fazal et al., 2017). NOTCH1 has been found to have a complex and extensive regulatory function in SCs. Studies in mouse mutants with conditional activation or inactivation of NOTCH1 signaling at different stages of the SC lineage showed that NOTCH1 promotes proliferation of immature SCs and triggers demyelination in injured nerves and in demyelinating neuropathies (Woodhoo et al., 2009). NOTCH1 is also necessary to maintain and control the SC repair phenotype, along with other transcription factors, like C-JUN and pathways like Raf/ERK (Jessen and Mirsky, 2008). It has been also shown to have a crucial role during the early stage of neural regeneration in the proximal nerve stump of injured peripheral nerve (Zhang et al., 2017).

Clusters of cis-regulatory elements (COREs) are reminiscent of super-enhancers, which are large clusters of active enhancers that drive gene expression and confer specific cell identity (Hnisz et al., 2013). We identified COREs with high TF activity, suggesting that these are hubs for transcriptional regulation. These CORES form long range interactions with promoters of genes that belong to the mTOR, AKT, AMPK and protein translation pathways. Expression of the AS-RNA induces significant change in expression of 15% of the gene families whose promoters form long range interactions with active COREs suggesting that the *EGR2*-AS-RNA may modulate part of the transcriptional programs regulating SC identity.

Areas of the genome where chromatin interactions are more frequent are termed "topologically associating domains" (TADs) (Dixon et al., 2012; Rao et al., 2014) (Figure S4). The positions of TADs within the genome are stable between several cell types and even across species (Nora et al., 2012; Schmitt et al., 2016) suggesting that TADs are architectural units that house regulatory interactions. Recent work has shown the existence of a certain hierarchy with TADs where domains are included within other domains (meta-TADs) through TAD-TAD interactions (An et al., 2019; Fraser et al., 2015) and this level of organization correlates with cell specific transcriptional and epigenetic regulation (Figure S4C). However, the molecular mechanisms that regulate this cell-specific architecture are not known. In addition, the possibility that changes in TAD-TAD interaction frequencies could have profound effects on cell identity programs open exciting possibilities for understanding and even modifying cell specific responses. To gain insight into the potential role of the *EGR2* promoter AS-RNA in modulating interactions between different TADs, we focused on the CORE-promoter interaction of *mTOR* since this CORE has all attributes of a regulatory hub.

Low resolution analysis of our Hi-C data following expression of the *EGR2*-AS-RNA shows that the promoter of *mTOR* and its regulatory COREs are positioned in separate TADs and form three distinct loop contacts. Expression of the AS-RNA significantly increases TF activity of AP-1, FOX, Tryptophan class, RHR class and GLI families that form TF communities on the inter-TAD contact boundaries between *mTOR* promoter and its COREs. In addition, expression of the AS-RNA induces formation of a new boundary at the *mTOR* gene that insulates *mTOR* from other intra or inter TAD interactions. The role of *mTOR* varies on SCs depending on the cellular state: it is crucial for myelination/differentiation of SCs during development (Norrmén and Suter, 2013; Norrmén et al., 2014), but in adulthood mTOR has been proposed to contribute to SCs remarkable

plasticity (Beirowski et al., 2017; Jiang et al., 2018). It has also been described as one of the first proteins that are upregulated after nerve injury, promoting C-JUN elevation and SC dedifferentiation (Norrmén and Suter, 2018).

We propose here that promoter AS-RNAs function as molecular scaffolds to recruit histone marks and may regulate interdomain regulatory hubs that are cell specific and, in the case of SCs, define molecular programs of cellular plasticity. Our results raise some intriguing possibilities and interesting mechanistic questions. Are these meta-TAD interactions formed by chromatin folding on single cells or are they results of aggregate populations of cells? Single-allele chromatin interactions do reveal regulatory hubs (Oudelaar et al., 2018), supporting the notion that these interactions occur in individual cells. What directs the binding of AS-RNA-histone mark complexes on specific TADs housing regulatory hubs? The presence of large communities of TFs with high binding activity suggests that there is cross-talk between TF regulation and promoter AS-RNA production. The possibility of TF feedback regulation of the promoter AS-RNA should be explored, and it could explain cell specific autonomous regulation. Finally, the ability of the *EGR2* promoter AS-RNA to regulate spatial genome architecture and transcriptional program of cell plasticity in SCs opens exciting possibilities for development of RNA therapeutics targeting promoter AS-RNAs for nerve regeneration.

Acknowledgements

This work was supported by a Warren Alpert Foundation grant (Project #17775) and internal funds of the Neurosurgery Department to N.T. Part of this work was facilitated by the Brown University Genomics Core.

Author Contributions

Conceptualization, N.T.; Investigation, M.M-M, and K.F.; Computational analysis, D.K., H.H., J.-S.C, E.F., and A.F.; Figures Generation, M.M.-M., D.K., H.H. and N.T.; Writing – Original Draft, M.M.-M., D.K. and N.T.; Writing – Review and Editing, N.T.; Funding Acquisition, N.T.; Resources, N.T.; Supervision, N.T.

Declaration of Interests

The authors declare no conflict of interest.

Figure legends

Figure 1: Expression of the *EGR2*-AS-RNA in SCs results in gene expression changes: (A) RNA-seq reveals an average of 2200 reads on the *EGR2* promoter following expression of the *EGR2*-AS-RNA. Control Schwann cells (Lenti-GFP) show an average of 240 reads on the *EGR2* promoter site. The RNA-seq experiments was performed in two biological replicates. (B) Volcano plot showing log-Fold Changes in gene expression following expression of the *EGR2*-AS-RNA in Schwann cells. 450 genes were significantly upregulated and 111 downregulated compared to control Schwann cells. (C) Clustering of upregulated and downregulated genes in Schwann cells expressing the *EGR2*-AS-RNA compared to control Schwann cells (n=2). The downregulated genes are enriched for ERK1/2, ERBB and MAPK regulated biological processes, while the upregulated genes are enriched in cell cycle regulators and mTOR regulated processes. (D) Expression of the *EGR2*-AS-RNA in Schwann cells results in increased protein expression of C-JUN and inhibition of the EGR2 protein expression. Significance was calculated with a Student's t-test (For EGR2, N = 8, 3 independent experiments, **p = 0.0017, dF = 7; For C-JUN, N = 10, 4 independent experiments, **p = 0.0016, dF = 18).

Figure 2: The *EGR2*-AS-RNA recruits EZH2 and WDR5 and enables coordinate targeting of H3K27me3 and H3K4me3 on *EGR2* and *C-JUN* promoters (A) RIP and ChIP experiments after the *EGR2*-AS-RNA overexpression in SCs, with antibodies against EZH2 and WDR5, and its effect to H3K27me3 on *EGR2* promoter and H3K4me3 on C-JUN promoter, respectively. Significance was calculated with a Student's t-test (For the WDR5 RIP, N = 13, 5 biological replicates, *p = 0.040, dF = 27; For the EZH2 RIP, N = 9, 3 biological replicates, *p = 0.026, dF = 16; For the H3K27me3 ChIP, N = 13, 5 biological replicates and 1 technical replicate, *p = 0.020, dF = 23, **p = 0.0094, dF = 22; For the H3K4me3 ChIP, N = 15, 5 biological replicates and 1 technical replicate, *p = 0.049, dF = 18, **p = 0.0012, dF = 23). (B) Western blotting showing the lack of interaction between WDR5 and EZH2 after WDR5 overexpression followed by FLAG IP. As an input control, we performed EZH2 Western blotting before the IP. Actin was used as a loading control on the Western blot and as a purity control of the IP. (C) RIP showing the preferential binding of the two portions of the antisense, AS1 or 5' portion to EZH2, and AS2 or 3' portion to WDR5 (All results were normalized with the empty plasmid control. For the AS1 RIP, N = 8, all biological replicates, *p = 0.043, dF = 14; For the AS2 RIP, N = 8, all biological replicates, *p = 0.010, dF = 10). (D) Schematic showing that the *EGR2* promoter AS-RNA functions as scaffold to coordinately recruit EZH2 and WDR5 on the promoters of *EGR2* and *c-JUN*. (E) Overexpression of the *EGR2*-AS-RNA increases the C-JUN DNA binding activity compared to the control (N = 5/group, 3 independent experiments, *p = 0.0176, dF = 10).

Figure 3: Expression of the *EGR2*-AS-RNA induces chromatin remodeling and increased activity of the AP-1/JUN TF family

A) Sample correlation analysis based on ATAC-seq peak location and intensity. PCA result of all samples is plotted as a 2D graph with PC1 as X-axis and PC 2 as Y-axis. Note that variable 1 is

strong (98%) to divide into the 2 hierarchical groups. (B) Scatterplot comparing ATAC-seq signal intensities across all open chromatin sites between the LentiAS group compared to the LentiGFP group. Significant changes correspond to an FDR-adjusted P value below 0.05 and an absolute log2 fold change above 1.5. The diagonal is shown as a gray area, as a reference indicating regions with no change in chromatin accessibility. Colored dots indicated differences in accessibility. (C) GO analysis among genes located in the vicinity of regions with increased chromatin accessibility after the *EGR2*-AS-RNA overexpression. (D) IGV of the mapped region relative to the c-Jun gene, shows more accessibility on the promoter on the LentiAS groups compared to LentiGFP. The position coordinates on the chromosome 5 is marked on the below line. The position and depth of mapped reads with the range are indicated at the left. (E and F) Volcano plot showing differential binding shown as footprint score versus the significance (logpval) shows differentially accessible by these TF pathways (E) and the TF itself (F) after the *EGR2*-AS-RNA OE in Schwann cells.

Figure 4: Hi-C following expression of the *EGR2*-AS-RNA in SCs shows reorganization of the global chromatin landscape

(A - C) Histogram showing the significant total loops called by the HiC+ software. Static loops (not gained or lost) are colored gray, lost loops are colored green and gained loops red (log2FC cutoff = 1, pvalue < 0.05). (D) Detail of the Hi-C maps on the chromosomes 10, 5 and 14 showing examples of gained, lost and static loops respectively. The annotated loop anchors to the promoter of genes are represented by their main pathways (plotted as odds ratios by their corresponding p values).

Figure 5: Reconstruction of long-range interactions between Cis-regulatory elements (COREs) and associated promoters in Schwann cells.

A) Schematic of clusters of regulatory elements (COREs) from accessibility data (ATAC-seq). Clusters of multiple proximal cis regulatory elements (CREs) were used to define COREs. Interacting COREs and promoters were annotated to loop anchors. B) Sub-setting of COREs based on transcription factor binding. 40% of COREs are occupied by at least 1 TF footprint. C) Hi-C reveals 192 unique COREs-promoter loops. 157 of 1563 COREs form long distance interaction with promoters. D) Example of COREs-promoter interactions at a genomic region at chromosome 20. COREs are colored by samples, red and blue for antisense OE and GFP control OE, respectively. Reference genome is color coded for expressed and non-expressed genes, respectively black and grey E) Depiction of loop interactions between a distant promoter and its associated COREs. Pathway enrichment analysis of COREs interacting genes. F) Volcano plot of differentially expressed COREs interacting genes following expression of the *EGR2*-AS-RNA (padj > 0.05, FC>1 or <1).

Figure 6: Ectopic expression of *EGR2* promoter AS-RNA results in changes between the mTOR promoter and its cis-regulatory elements.

a) Depicts the three contact points completely overlapping COREs and mTOR promoter. Magnification of the COREs region with anchors in blue with detailed coordinate characterization of the region. Characteristic of loop anchor region overlapping the COREs region. "Nearest/mid/farthest" distance to TAD boundary nomenclature denotes the three loop anchors position within the TAD in relation to the closest boundary. COREs are colored by samples, red and blue for antisense OE and GFP control OE, respectively. Reference genome is color coded by expressed and non-expressed genes, respectively black and grey in color. mTOR shown in blue in

gene reference panel. b) Change in TF binding activity/binding scores of all TFs at nearest and mid distance to TAD boundary loop anchors following promoter antisense OE (farthest to TAD boundary loop anchor could not be analyzed due to very low occupancy). c) Prediction of TF families that experience the greatest increase in activity/binding scores following promoter antisense OE.

Figure 7: Network prediction of TF activity dynamics at the mTOR interacting regulatory element/super enhancer.

A) Network of TF activity at the loop interacting with the COREs at the nearest TAD boundary. B) Network of TF activity at the loop interacting with the COREs at the mid distance to the TAD boundary. C) Network of TF activity at the loop interacting with the COREs farthest to the TAD boundary. Maroon color emphasizes TF class and families that experience a statistically significant increase in TF activity following expression of the *EGR2*-AS-RNA (Wilcoxon test, p-val <0.05).

Figure 8: *EGR2*-AS-RNA induces structural reorganization and TF activity changes at the mTOR interdomain regulatory hub.

A) Depiction of mTOR interaction hub harboring meta-TAD. Tracks shown below (from top to bottom): clusters of cis-regulatory elements (COREs), genomic loops, active/inactive compartments, ATAC-seq reads, RNA-seq reads for individual replicates. B) Proposed model of 2D interdomain interactions between COREs and mTOR promoter. Magnified depiction of activity at hub shown with blue intensity. C) Depiction of changes at mTOR harboring TAD. D) bar-plots of normalized gene expression in lentiGFP and lentiAS (FC=1.28, p.adj = 0.03).

Figure 1

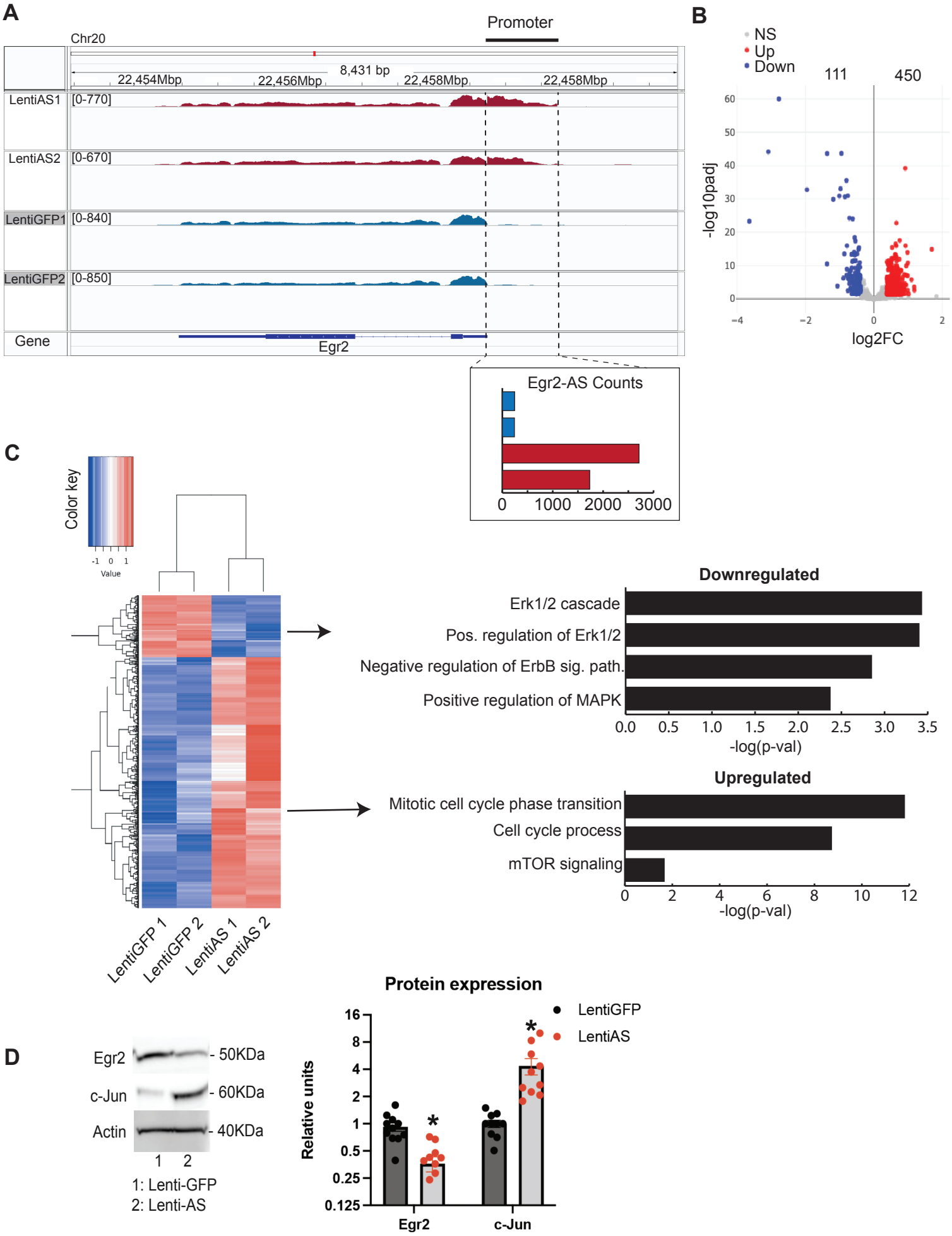
A
Promoter
Chr20
8,431 bp
22,454Mbp
22,456Mbp
22,458Mbp
22,458Mbp
LentiAS1
[0-770]
LentiAS2
[0-670]
LentiGFP1
[0-840]
LentiGFP2
[0-850]
Gene
Egr2
Egr2-AS Counts
0
1000
2000
3000
B
NS
Up
Down
111
450
-log10padj
log2FC
C
Color key
Value
LentiGFP 1
LentiGFP 2
LentiAS 1
LentiAS 2
Downregulated
Erk1/2 cascade
Pos. regulation of Erk1/2
Negative regulation of ErbB sig. path.
Positive regulation of MAPK
-log(p-val)
Upregulated
Mitotic cell cycle phase transition
Cell cycle process
mTOR signaling
-log(p-val)
D
Egr2
- 50KDa
c-Jun
- 60KDa
Actin
- 40KDa
1 2
1: Lenti-GFP
2: Lenti-AS
Protein expression
LentiGFP
LentiAS
Relative units
Egr2
c-Jun

Figure 2

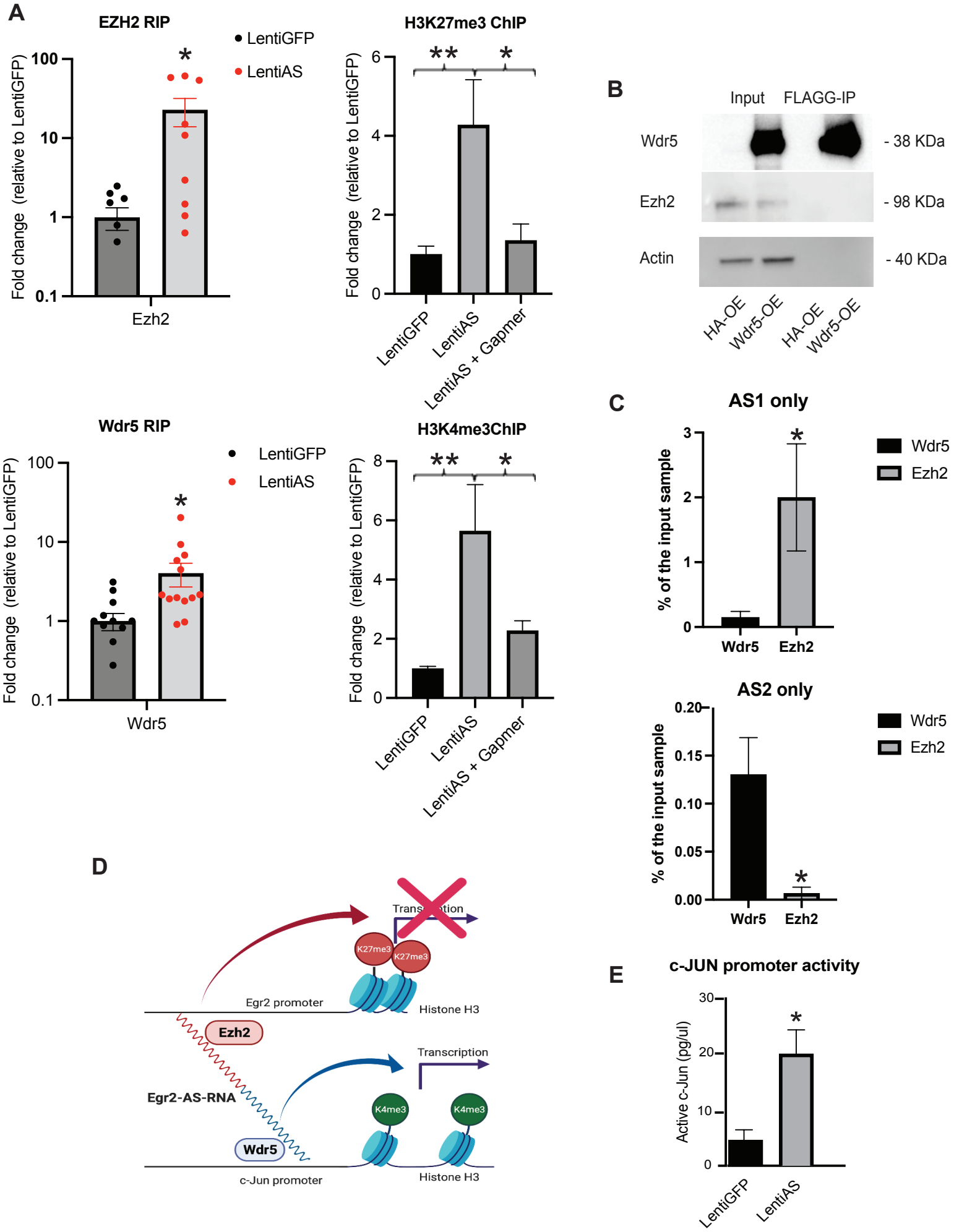
A
EZH2 RIP
LentiGFP
LentiAS
Fold change (relative to LentiGFP)
100
10
1
0.1
*
Ezh2
H3K27me3 ChIP
**
*
6
4
2
0
LentiGFP
LentiAS
LentiAS + Gapmer
Wdr5 RIP
Wdr5
H3K4me3ChIP
B
Input
FLAGG-IP
Wdr5
Ezh2
Actin
- 38 KDa
- 98 KDa
- 40 KDa
HA-OE
Wdr5-OE
C
AS1 only
% of the input sample
Wdr5
Ezh2
AS2 only
0.20
0.15
0.10
0.05
0.00
D
Transcription
K27me3
Egr2 promoter
Histone H3
Ezh2
Egr2-AS-RNA
K4me3
Wdr5
c-Jun promoter
E
c-JUN promoter activity
Active c-Jun (pg/ul)
30
20
10
0

Figure 3

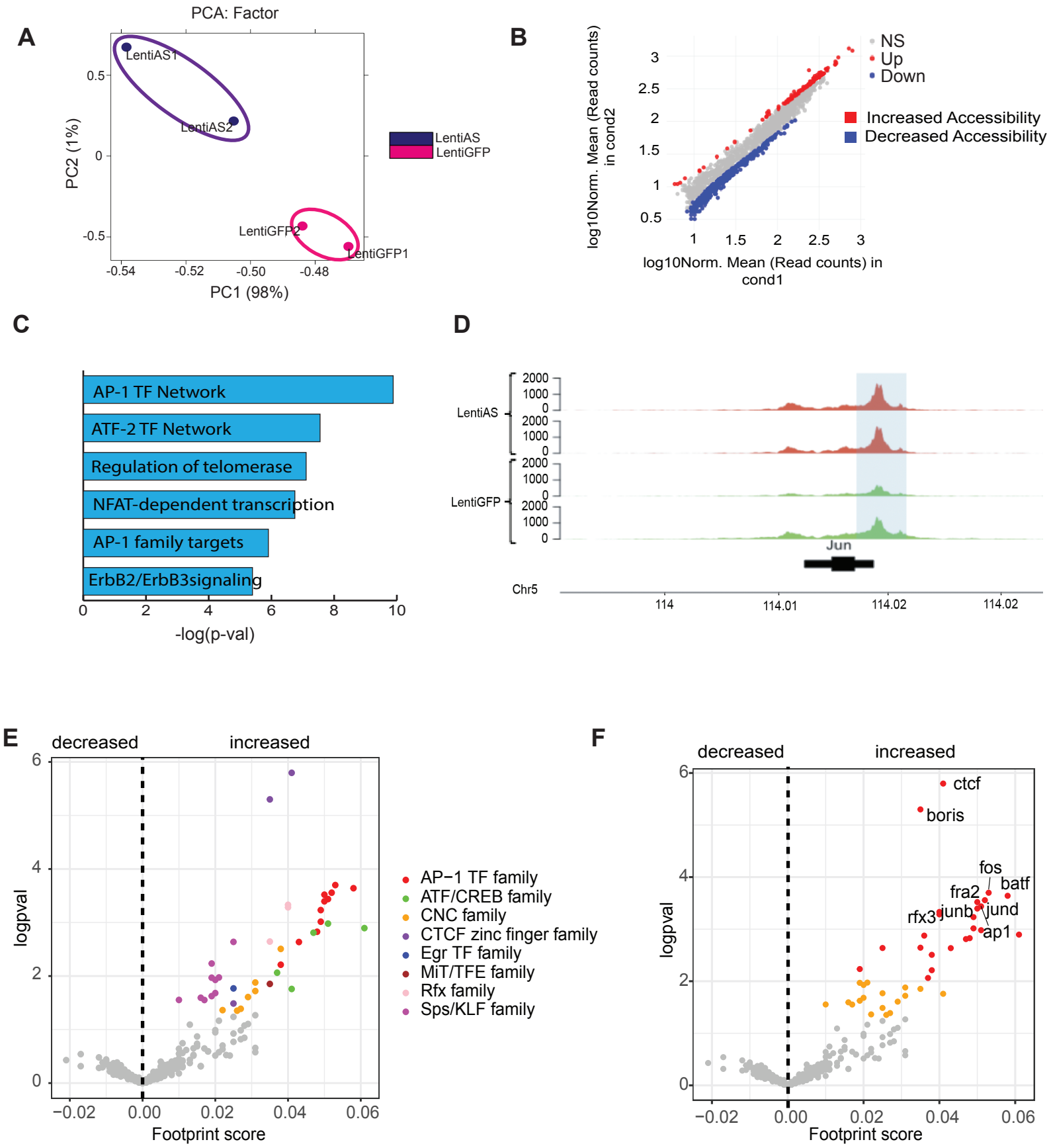
A
PCA: Factor
LentiAS1
LentiAS2
LentiGFP2
LentiGFP1
PC2 (1%)
PC1 (98%)
LentiAS
LentiGFP
B
NS
Up
Down
Increased Accessibility
Decreased Accessibility
log10Norm. Mean (Read counts) in cond2
log10Norm. Mean (Read counts) in cond1
C
AP-1 TF Network
ATF-2 TF Network
Regulation of telomerase
NFAT-dependent transcription
AP-1 family targets
ErbB2/ErbB3signaling
-log(p-val)
D
LentiAS
LentiGFP
Jun
Chr5
114
114.01
114.02
114.02
E
decreased
increased
logpval
Footprint score
AP−1 TF family
ATF/CREB family
CNC family
CTCF zinc finger family
Egr TF family
MiT/TFE family
Rfx family
Sps/KLF family
F
decreased
increased
ctcf
boris
fos
batf
fra2
junb
jund
rfx3
ap1
logpval
Footprint score

Figure 4

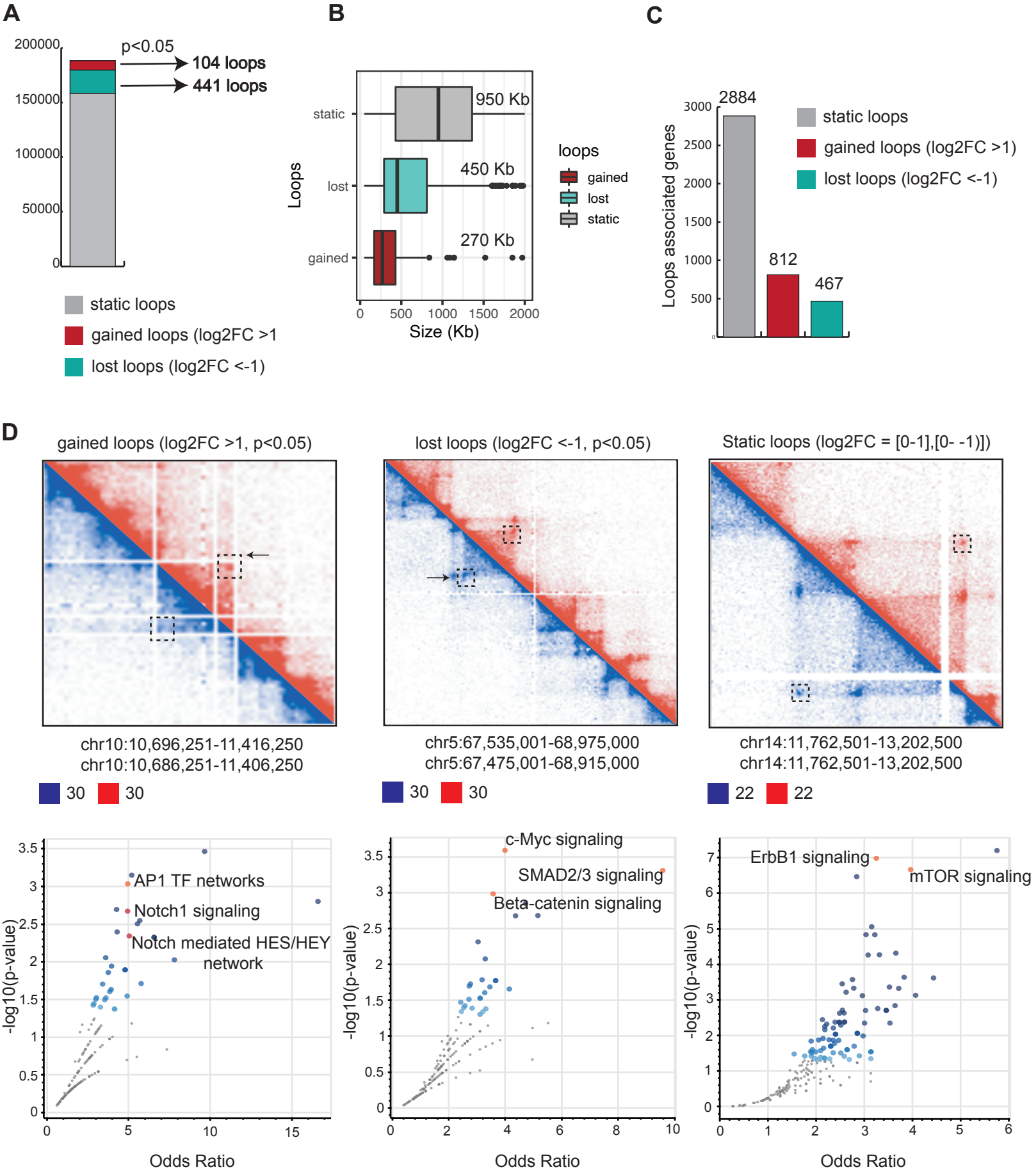
A
200000
150000
100000
50000
0
p<0.05
104 loops
441 loops
static loops
gained loops (log2FC >1
lost loops (log2FC <-1)
B
static
lost
gained
Loops
950 Kb
450 Kb
270 Kb
0
500
1000
1500
2000
Size (Kb)
loops
gained
lost
static
C
Loops associated genes
3000
2500
2000
1500
1000
500
2884
812
467
static loops
gained loops (log2FC >1)
lost loops (log2FC <-1)
D
gained loops (log2FC >1, p<0.05)
chr10:10,696,251-11,416,250
chr10:10,686,251-11,406,250
30
30
lost loops (log2FC <-1, p<0.05)
chr5:67,535,001-68,975,000
chr5:67,475,001-68,915,000
30
30
Static loops (log2FC = [0-1],[0- -1)])
chr14:11,762,501-13,202,500
chr14:11,762,501-13,202,500
22
22
-log10(p-value)
AP1 TF networks
Notch1 signaling
Notch mediated HES/HEY network
Odds Ratio
c-Myc signaling
SMAD2/3 signaling
Beta-catenin signaling
Odds Ratio
ErbB1 signaling
mTOR signaling
Odds Ratio

Figure 5

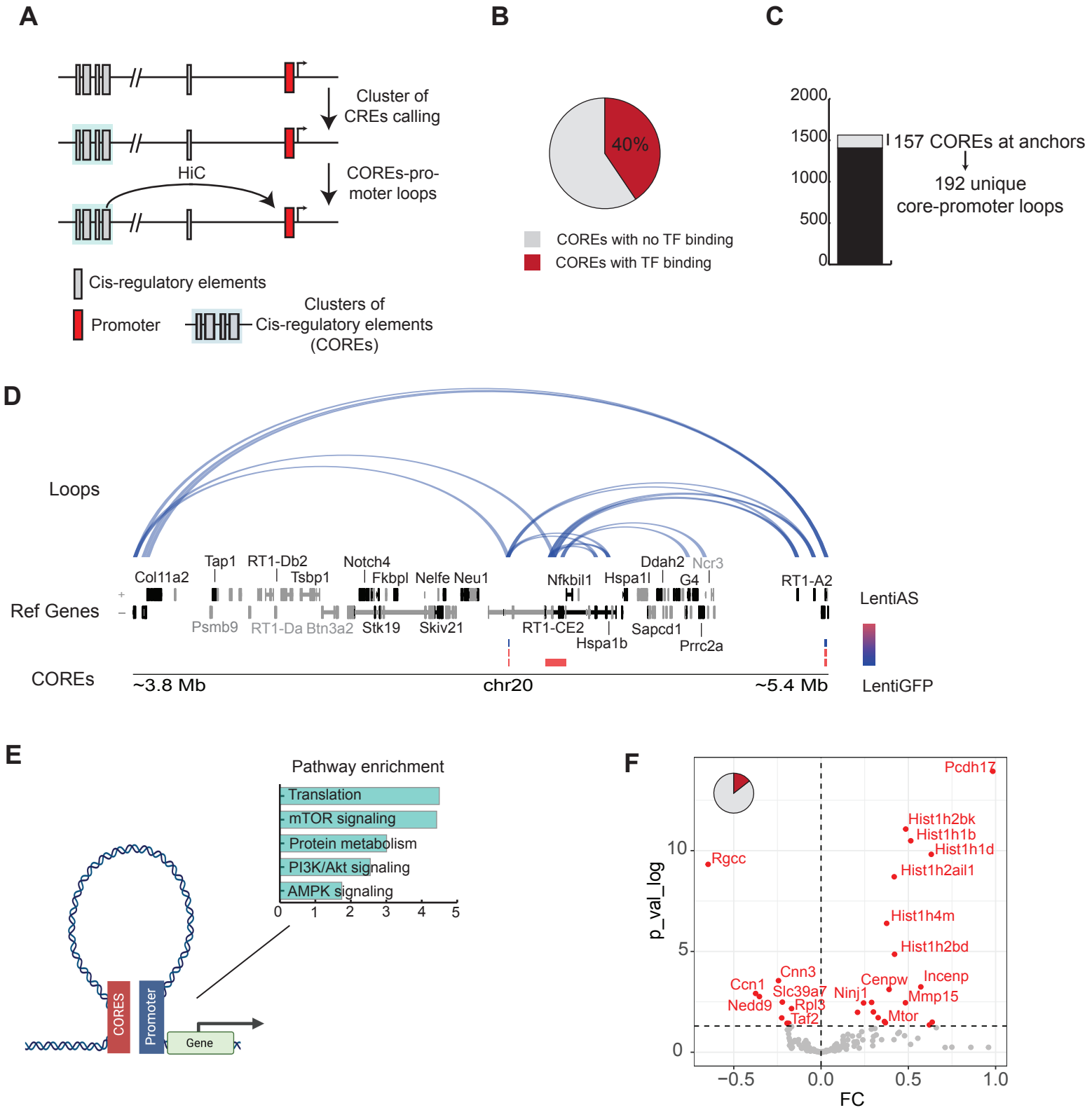
A
Cluster of CREs calling
HiC
COREs-promoter loops
Cis-regulatory elements
Promoter
Clusters of Cis-regulatory elements (COREs)
B
40%
COREs with no TF binding
COREs with TF binding
C
2000
1500
1000
500
0
157 COREs at anchors
192 unique core-promoter loops
D
Loops
Ref Genes
COREs
Col11a2
Tap1
RT1-Db2
Tsbp1
Notch4
Fkbpl
Nelfe
Neu1
Nfkbil1
Hspa1l
Ddah2
Ncr3
G4
RT1-A2
Psmb9
RT1-Da
Btn3a2
Stk19
Skiv21
RT1-CE2
Hspa1b
Sapcd1
Prrc2a
~3.8 Mb
chr20
~5.4 Mb
LentiAS
LentiGFP
E
Pathway enrichment
Translation
mTOR signaling
Protein metabolism
PI3K/Akt signaling
AMPK signaling
0
1
2
3
4
5
CORES
Promoter
Gene
F
Pcdh17
Hist1h2bk
Hist1h1b
Hist1h1d
Rgcc
Hist1h2ail1
Hist1h4m
Hist1h2bd
Cnn3
Ccn1
Slc39a7
Nedd9
Rpl3
Taf2
Cenpw
Incenp
Ninj1
Mmp15
Mtor
p_val_log
10
5
0
−0.5
0.0
0.5
1.0
FC

Figure 6

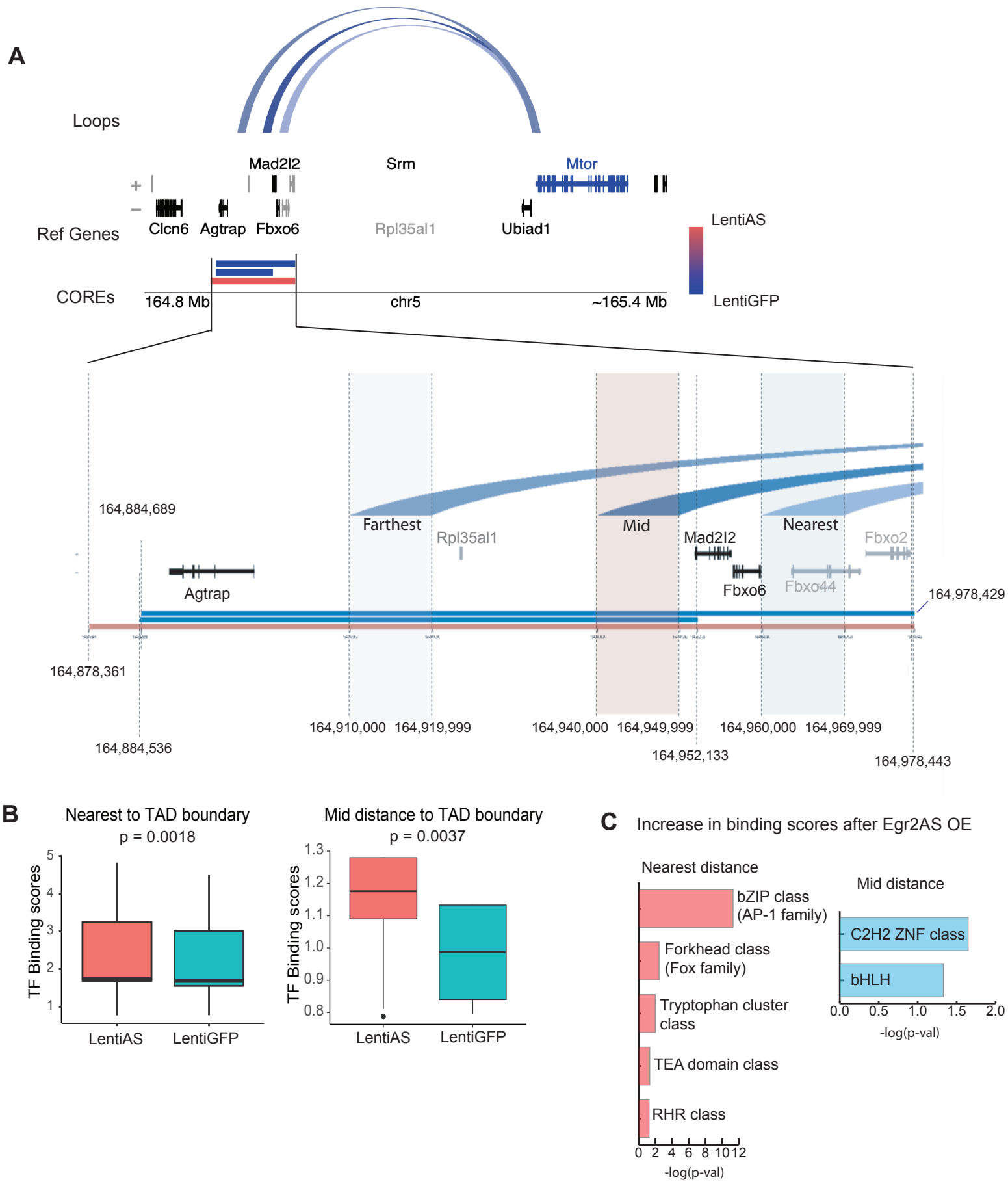
A
Loops
Mad2l2
Srm
Mtor
Ref Genes
Clcn6
Agtrap
Fbxo6
Rpl35al1
Ubiad1
LentiAS
LentiGFP
COREs
164.8 Mb
chr5
~165.4 Mb
164,884,689
Farthest
Rpl35al1
Mid
Mad2l2
Nearest
Fbxo2
Agtrap
Fbxo6
Fbxo44
164,978,429
164,878,361
164,884,536
164,910,000
164,919,999
164,940,000
164,949,999
164,960,000
164,969,999
164,952,133
164,978,443
B
Nearest to TAD boundary
p = 0.0018
TF Binding scores
LentiAS
LentiGFP
Mid distance to TAD boundary
p = 0.0037
TF Binding scores
LentiAS
LentiGFP
C
Increase in binding scores after Egr2AS OE
Nearest distance
bZIP class (AP-1 family)
Forkhead class (Fox family)
Tryptophan cluster class
TEA domain class
RHR class
-log(p-val)
Mid distance
C2H2 ZNF class
bHLH
-log(p-val)

Figure 7

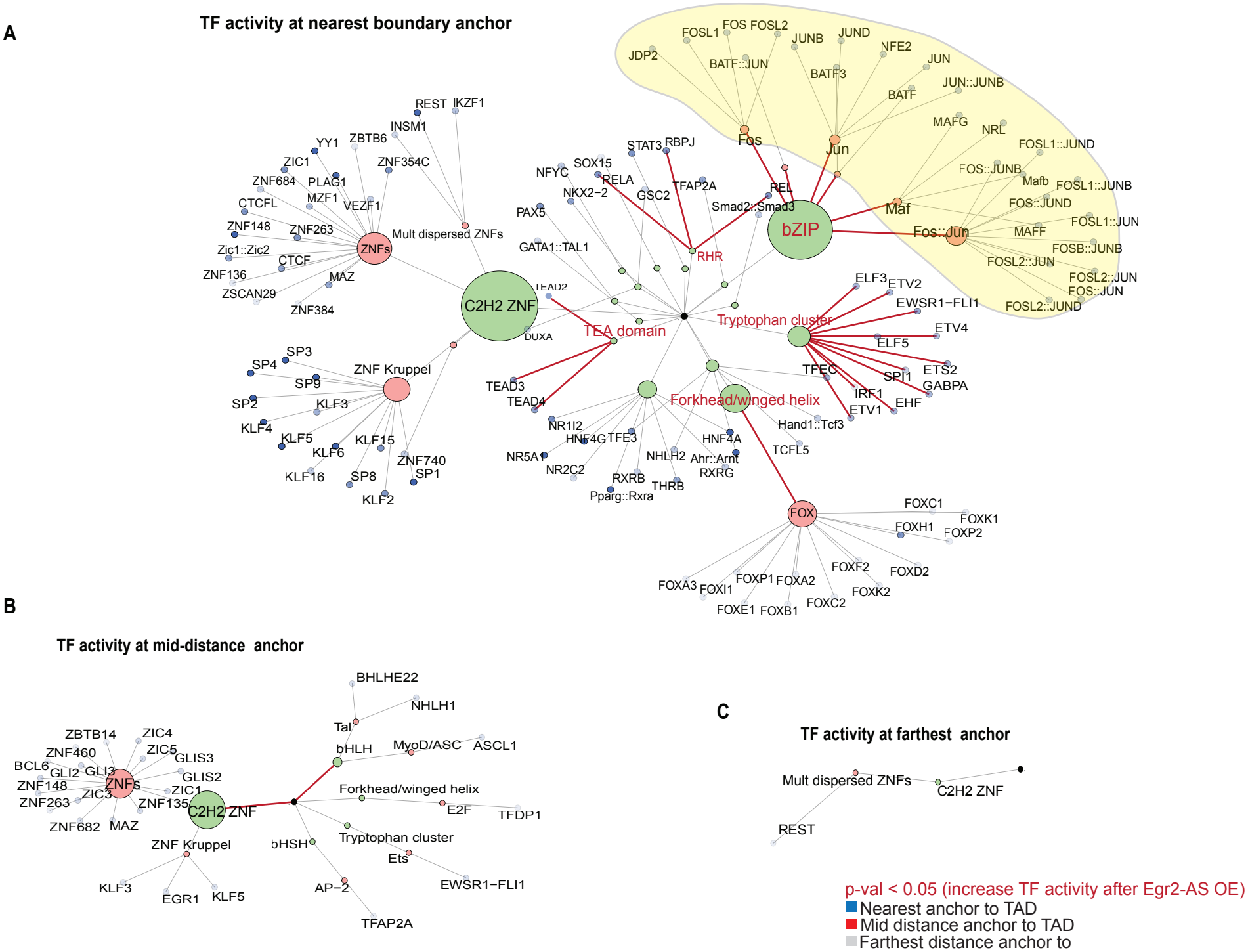
A
TF activity at nearest boundary anchor
REST
IKZF1
INSM1
YY1
ZBTB6
ZIC1
ZNF354C
ZNF684
PLAG1
MZF1
CTCFL
VEZF1
ZNF148
ZNF263
Zic1::Zic2
CTCF
ZNF136
MAZ
ZSCAN29
ZNF384
ZNFs
Mult dispersed ZNFs
C2H2 ZNF
TEAD2
DUXA
SP3
SP4
SP9
SP2
KLF3
KLF4
KLF5
KLF6
KLF15
KLF16
SP8
ZNF740
SP1
KLF2
ZNF Kruppel
TEAD3
TEAD4
TEA domain
NR1I2
HNF4G
TFE3
NR5A1
NR2C2
NHLH2
RXRB
THRB
Pparg::Rxra
Ahr::Arnt
RXRG
HNF4A
TCFL5
Forkhead/winged helix
Hand1::Tcf3
FOX
FOXC1
FOXK1
FOXH1
FOXP2
FOXF2
FOXD2
FOXA3
FOXI1
FOXP1
FOXA2
FOXK2
FOXE1
FOXB1
FOXC2
STAT3
RBPJ
NFYC
SOX15
RELA
NKX2−2
GSC2
TFAP2A
PAX5
GATA1::TAL1
RHR
REL
Smad2::Smad3
bZIP
Tryptophan cluster
ELF3
ETV2
EWSR1−FLI1
ETV4
ELF5
TFEC
SPI1
ETS2
GABPA
IRF1
EHF
ETV1
JDP2
FOSL1
FOS
FOSL2
JUNB
JUND
NFE2
BATF::JUN
BATF3
JUN
JUN::JUNB
BATF
MAFG
NRL
Fos
Jun
FOSL1::JUND
FOS::JUNB
Mafb
FOSL1::JUNB
FOS::JUND
Maf
FOSL1::JUN
Fos::Jun
MAFF
FOSB::JUNB
FOSL2::JUN
FOSL2::JUN
FOS::JUN
FOSL2::JUND
B
TF activity at mid-distance anchor
BHLHE22
NHLH1
Tal
bHLH
MyoD/ASC
ASCL1
ZBTB14
ZIC4
ZNF460
ZIC5
GLIS3
BCL6
GLI2
GLI3
GLIS2
ZNF148
ZNFs
ZIC1
ZNF263
ZIC3
ZNF135
C2H2 ZNF
ZNF682
MAZ
Forkhead/winged helix
E2F
TFDP1
ZNF Kruppel
bHSH
Tryptophan cluster
Ets
KLF3
EGR1
KLF5
AP−2
EWSR1−FLI1
TFAP2A
C
TF activity at farthest anchor
Mult dispersed ZNFs
C2H2 ZNF
REST
p-val < 0.05 (increase TF activity after Egr2-AS OE)
Nearest anchor to TAD
Mid distance anchor to TAD
Farthest distance anchor to

Figure 8

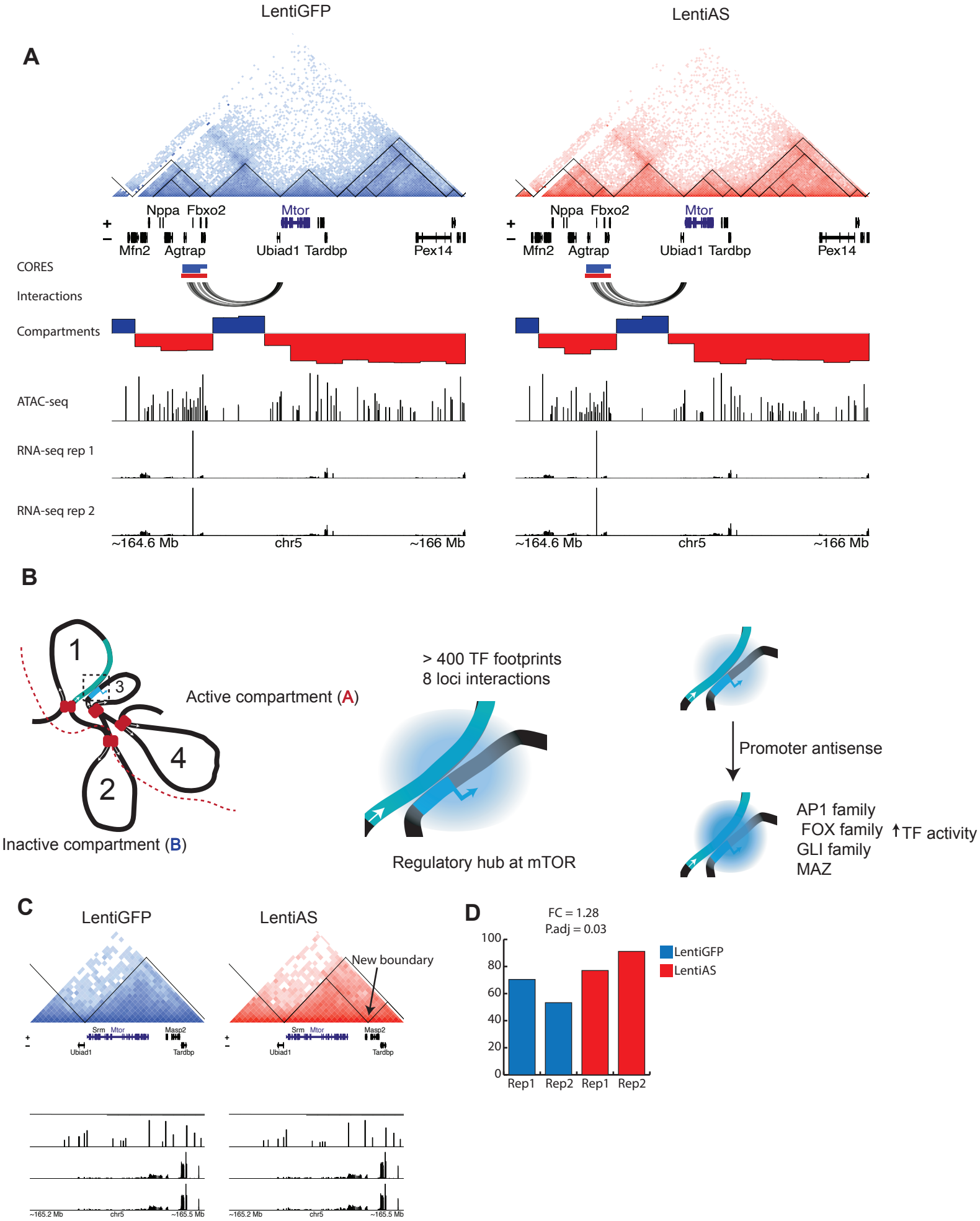
A
LentiGFP
LentiAS
Nppa Fbxo2
Mtor
Mfn2 Agtrap
Ubiad1 Tardbp
Pex14
CORES
Interactions
Compartments
ATAC-seq
RNA-seq rep 1
RNA-seq rep 2
~164.6 Mb
chr5
~166 Mb
B
1
2
3
4
Active compartment (A)
Inactive compartment (B)
> 400 TF footprints
8 loci interactions
Regulatory hub at mTOR
Promoter antisense
AP1 family
FOX family
GLI family
MAZ
TF activity
C
LentiGFP
LentiAS
New boundary
Srm Mtor
Masp2
Ubiad1
Tardbp
~165.2 Mb
chr5
~165.5 Mb
D
FC = 1.28
P.adj = 0.03
100
80
60
40
20
0
Rep1 Rep2 Rep1 Rep2
LentiGFP
LentiAS

STAR Methods

Methods for Schwann cell cultures, Western Blotting, Immunoprecipitations, Transfections, qPCR, Cloning, TF activity assays and Primer sequences are included in the Supplemental Information.

RNA-seq

Sequencing reads were aligned to the rn6 genome assembly with hisat2 (Should this be hisat2 instead of hista2?) (Kim et al., 2019). Gene-wise read summarization was done with featureCounts using Refseq exon coordinates as specified in the rn6 refGene file available in the UCSC Genome Browser database (Lee et al., 2022; Liao et al., 2014). Differential gene expression analysis was done in R via DEBrowser the DESeq2 platform (Kucukural et al., 2019; Love et al., 2014). We used an adjusted p-value cut-off of 0.05 and a fold change of 1.3.

ATAC-seq

Sequencing reads were aligned to the rn6 genome assembly with bowtie2, and duplicate reads were removed with picard-tools (Picard Toolkit, 2019; Langmead and Salzberg, 2012). Promoters were defined as 2000 bp regions positioned between -1500 to +500 nucleotides with respect to the transcription start site, as annotated in Refseq. Peaks of chromatin accessibility were detected using MACS2, and those located at promoter regions were identified using the intersectBed command in BEDtools (previously "intersectBed routine of Bedtools"). (Quinlan and Hall, 2010; Zhang et al., 2008). To compare relative promoter accessibility, ATAC reads mapping promoters were quantified with featureCounts and the promoter locations defined above. Differential promoter accessibility was determined with the limma package (Ritchie et al., 2015). A p-adjusted value of 0.05 and fold change of 1.5 were used as cut-offs.

RNA immunoprecipitation (RIP)

To perform RIP, we used the magnetic RNA ChIP kit. Briefy, cells were subjected to crosslinking in 1% formaldehyde in PBS, then lysed in the kit-provided lysis buffer, and then, after centrifugation, the pellet that contained the chromatin was sheared to 100-1000 bp (the settings of the sonicator depend on the cell type or tissue type). Sheared chromatin was subjected to DNAse treatment and then we proceeded to the immunoprecipitation with the magnetic beads. For each immunoprecipitation, we added 10 µg of sheared chromatin and 1 µg of ChIP grade antibody (list of antibodies in table 2) and an isotype control for unspecific binding to the magnetic beads. Then we incubated the tubes to an end-to-end rotator overnight at 4ºC. Then, we eluted the RNA and proteins, degraded the proteins with Proteinase K and reversed the crosslinks. We purified the RNA doing a Trizol extraction and performed qPCR against AS-Egr2 RNA. Relative enrichment for each experimental sample was calculated as a percentage of the input, and the isotype control percentage was deducted from each experimental condition.

Chromatin Immunoprecipitation (ChIP)

For DNA Chromatin Immunoprecipitation (ChIP) we used the ChIP-IT High Sensitivity® kit from Active motif. Lysates were obtained as described in the RIP protocol. Lysates were incubated overnight at 4ºC on rotation with the specific ChIP-verified antibodies (list on table 2). For negative control ChIP, we used a non-targeting isotype-matched IgG. Chromatin was then precipitated, and DNA was extracted. Recovered material from the input sample and all the ChIP samples per condition were used to perform qPCR of the Egr2-AS-RNA. Calculations were performed as the RIP experiments.

Hi-C capture method

Hi-C was performed using the Arima-HiC kit. As per their protocol, we tested the amount of input sample beforehand and we used 2 million cells per each independent sample. We did QC on samples in every recommended step. Sonication was performed using the Covaris s220 instrument to a fragment size of 300-400 bp (Settings: Power: 5, Duty Factor: 10%, Cycles per Burst: 200, and Time: 60 sec per process). We used KAPA Hyper Prep Kit to generate libraries. The primers used for indexing were obtained from Illumina, and the libraries were quantified and QC was done using the KAPA Library Quantification Kit. Libraries were sequenced by GENEWIZ using the Illumina HiSeq 2500 system to acquire 150 bp paired-end sequence reads, reaching 300M reads for each sample based on total usable reads >20 Kb.

Raw and ICE-normalized contact matrices were prepared with HiC-Pro (Servant et al., 2015). ICE-normalized and condition-merged HiC-Pro matrices were converted to Juicer .hic files for resolutions 10 Kb and 100 Kb using a wrapper for the Juicer tools Pre command in the HiC-DC+ Bioconductor package (Durand et al., 2016; Sahin et al., 2021).

Significant and differential loop analysis

Significant loops (q-value <= 0.05) and differential loops (log2FC cut-off = 1, p-value < 0.05) across conditions were identified using HiC-DC+ with raw HiC-Pro matrices and bed files of two AS replicates and two GFP replicates at 10 Kb resolution (Sahin *et al.*, 2021). To filter biases in denser genomic regions in close proximity and noise in sparser regions that are more far apart, only loops between 50 Kb and 2 Mb were called.

We categorized the loops into three sets: 1) static for significant loops that did not meet the differential loops thresholds, 2) dynamic gain for significant loops that were differential with a log2FC > 1, and 3) dynamic lost for significant loops that were differential with a log2FC < -1.

Dynamic loops represent interactions that, after antisense overexpression, were gained or lost relative to their interaction frequencies in GFP control samples.

Identification of clusters of cis-regulatory elements (COREs)

The R package CREAM version 1.1.1 was used to identify clusters of *cis*-regulatory elements, or COREs (Madani Tonekaboni *et al.*, 2019). The bed files for the peaks were used as an input and the program was run with parameters MinLength = 1000 and peakNumMin = 2 for all the LentiAS and LentiGFP samples.

Annotation/identification of COREs-promoter loops

Gene symbols obtained from the RNA-seq analysis were first mapped to stable rn6 Entrez Gene identifiers, then to transcripts, and finally to 2200 bp-width promoters using the Bioconductor packages TxDb.Rnorvegicus.UCSC.rn6.refGene, BSgenome.Rnorvegicus.UCSC.rn6, and org.Rn.eg.db (Carlson, 2019; Team and Maintainer, 2019; Team, 2019). We defined COREs-promoter loops as loops that consisted of one anchor intersecting with at least one promoter and the other anchor intersecting with at least one COREs. Anchors of COREs-promoter loops had at least a 1 bp-overlap with promoters or COREs. A subset of these loops had complete overlaps at anchors in which an entire promoter or COREs was contained in the 10 Kb loop anchor or, for COREs greater than 10 Kb in width, the entire loop anchor was contained in the COREs.

Genome wide differential TF activity at promoter sites

Peaks were annotated against the rn6 genome. The R package diffbind from Bioconductor was used to compare the similarity in peak read counts via correlation heatmaps and principal components analysis (Ross-Innes et al., 2012). The R package DESeq2 from Bioconductor was used to detect differential peak regions (Love *et al.*, 2014). To do so, a consensus set of peaks was first generated via the runConsensusRegions function in the *soGGi* package (Dharmalingam and

Carroll, 2015), and then read counts of each peak range in the consensus peak set were calculated via the featureCounts function in the Rsubread package for each sample (Dharmalingam and Carroll, 2015; Liao *et al.*, 2014; 2019). The resulting counts matrix was then processed via DESeq, and differentially accessible chromatin regions between control and experimental samples were defined as peak regions with an absolute fold change greater than 1.5 and a p-value less than 0.05. Genes associated with differentially accessible peaks were identified through a many-to-many mapping algorithm implemented in the seq2gene function from the ChIPseeker package (Yu et al., 2015). Promoters with differential accessibility were defined as differentially accessible peak regions within 3000 bp upstream and downstream of a TSS in the rn6 genome. DAStk was used to quantify significant differences in transcription factor activity at the differentially accessible promoter sites (Tripodi et al., 2018). Motif binding sites with differential activity were analyzed through EnrichR to identify enriched gene ontology categories (Kuleshov et al., 2016).

Site-specific TF footprint/binding predictions

TOBIAS was used to identify specific footprint location at DNA regulatory elements (Bentsen et al., 2020). First, the ATACorrect function was ran to correct for tn5 insertion bias. Next, depletion signal (negative counts) and general accessibility at surrounding regions were used to derive a binding score. Finally, to make TF binding activity predictions, the footprint scores were matched to binding motifs from the 2020 JASPAR CORE database (Fornes et al., 2020). TF binding activity were restricted to accessible loop anchor sites using genomic contact regions derived from Hi-C data. Finally, the exact sites predicted to be bound were extracted for further site-specific downstream analysis.

Site-specific TF binding predictions at regulatory elements

All intersections of TF footprints with anchors, promoters, and COREs had an overlap of at least 1 bp. We identified TF footprints that intersected with COREs and with all anchors overlapping with COREs. TF footprints that intersected with each of the three loop anchors interacting with the mTOR promoter (i.e. anchors containing COREs) were grouped into families and classes based on the 2020 and 2022 JASPAR CORE databases (Castro-Mondragon et al., 2022; Fornes *et al.*, 2020). To identify significant differences between AS and GFP footprint scores (binding scores) at each anchor, we performed Wilcoxon rank sum tests in R on 1) the full list of TF footprints that intersected with the loop anchor and were present in both AS and GFP samples and 2) the same list grouped by TF class.

Identification of TADs

The C++ software OnTAD was to detect hierarchical TADs in ICE normalized and condition-merged .hic files at 10 Kb resolution (An *et al.*, 2019). The OnTAD executable file was compiled under gcc 8.3 and run with default parameters.

Intra and inter TAD loops localization

We defined intra-TAD loops as loops with both anchors intersecting with the same outermost TAD and inter-TAD loops as loops with anchors intersecting with different outermost TADs. All intra- and inter-TAD loop anchors were annotated with genes with promoters that overlapped with any region of the anchor.

Identification of A/B Compartments

The eigenvector command in Juicer tools version 1.19.02 was used to call A/B compartments in ICE-normalized and condition-merged .hic files at 100 Kb resolution (Durand *et al.*, 2016). The signs of the output eigenvectors indicate the compartment, but the signs are arbitrary in each set of eigenvectors calculated for each chromosome and condition. Therefore, for regions of interest,

eigenvectors were plotted alongside ATAC-seq narrow peaks using the plotgardener R package to determine whether they corresponded to compartment A or B (Kramer et al., 2022).

Software & Data availability

Hi-C analysis scripts are available at https://github.com/hyeyeon-hwang/HiC-Analysis-of-Egr2-AS-RNA.

All datasets (RNA-seq, ATAC-seq, Hi-C) have been deposited to the GEO Omnibus and can be accessed through: https://www.ncbi.nlm.nih.gov/geo/query/acc.cgi?acc=GSE201627

Plasmid Availability

The lentivirus construct (LentiAS) is deposited to Addgene and is available to order (#177737).

References

Akhade, V.S., Pal, D., and Kanduri, C. (2017). Long Noncoding RNA: Genome Organization and Mechanism of Action. Adv Exp Med Biol *1008*, 47-74. 10.1007/978-981-10-5203-3_2.

An, L., Yang, T., Yang, J., Nuebler, J., Xiang, G., Hardison, R.C., Li, Q., and Zhang, Y. (2019). OnTAD: hierarchical domain structure reveals the divergence of activity among TADs and boundaries. Genome Biol *20*, 282. 10.1186/s13059-019-1893-y.

Arthur-Farraj, P.J., Latouche, M., Wilton, D.K., Quintes, S., Chabrol, E., Banerjee, A., Woodhoo, A., Jenkins, B., Rahman, M., Turmaine, M., et al. (2012). c-Jun reprograms Schwann cells of injured nerves to generate a repair cell essential for regeneration. Neuron *75*, 633-647. 10.1016/j.neuron.2012.06.021.

Beirowski, B., Wong, K.M., Babetto, E., and Milbrandt, J. (2017). mTORC1 promotes proliferation of immature Schwann cells and myelin growth of differentiated Schwann cells. Proc Natl Acad Sci U S A *114*, E4261-E4270. 10.1073/pnas.1620761114.

Bentsen, M., Goymann, P., Schultheis, H., Klee, K., Petrova, A., Wiegandt, R., Fust, A., Preussner, J., Kuenne, C., Braun, T., et al. (2020). ATAC-seq footprinting unravels kinetics of transcription factor binding during zygotic genome activation. Nat Commun *11*, 4267. 10.1038/s41467-020-18035-1.

Carlson, M. (2019). org.Rn.eg.db: Genome wide annotation for Rat. R package version 3.14.0.

Castro-Mondragon, J.A., Riudavets-Puig, R., Rauluseviciute, I., Berhanu Lemma, R., Turchi, L., Blanc-Mathieu, R., Lucas, J., Boddie, P., Khan, A., Manosalva Perez, N., et al. (2022). JASPAR 2022: the 9th release of the open-access database of transcription factor binding profiles. Nucleic Acids Res *50*, D165-D173. 10.1093/nar/gkab1113.

Cockerill, P.N. (2011). Structure and function of active chromatin and DNase I hypersensitive sites. FEBS J *278*, 2182-2210. 10.1111/j.1742-4658.2011.08128.x.

Dharmalingam, G., and Carroll, T. (2015). soGGi: Visualise ChIP-seq, MNase-seq and motif occurrence as aggregate plots Summarised Over Grouped Genomic Intervals. R package version 1.4.4.

Dixon, J.R., Selvaraj, S., Yue, F., Kim, A., Li, Y., Shen, Y., Hu, M., Liu, J.S., and Ren, B. (2012). Topological domains in mammalian genomes identified by analysis of chromatin interactions. Nature *485*, 376-380. 10.1038/nature11082.
Dowen, J.M., Fan, Z.P., Hnisz, D., Ren, G., Abraham, B.J., Zhang, L.N., Weintraub, A.S., Schujiers, J., Lee, T.I., Zhao, K., and Young, R.A. (2014). Control of cell identity genes occurs in insulated neighborhoods in mammalian chromosomes. Cell *159*, 374-387. 10.1016/j.cell.2014.09.030.
Duman, M., Martinez-Moreno, M., Jacob, C., and Tapinos, N. (2020). Functions of histone modifications and histone modifiers in Schwann cells. Glia *68*, 1584-1595. 10.1002/glia.23795.
Durand, N.C., Shamim, M.S., Machol, I., Rao, S.S., Huntley, M.H., Lander, E.S., and Aiden, E.L. (2016). Juicer Provides a One-Click System for Analyzing Loop-Resolution Hi-C Experiments. Cell Syst *3*, 95-98. 10.1016/j.cels.2016.07.002.
Fazal, S.V., Gomez-Sanchez, J.A., Wagstaff, L.J., Musner, N., Otto, G., Janz, M., Mirsky, R., and Jessen, K.R. (2017). Graded Elevation of c-Jun in Schwann Cells In Vivo: Gene Dosage Determines Effects on Development, Remyelination, Tumorigenesis, and Hypomyelination. J Neurosci *37*, 12297-12313. 10.1523/JNEUROSCI.0986-17.2017.
Figlia, G. (2018). c-Jun in Schwann Cells: Stay Away from Extremes. J Neurosci *38*, 3388-3390. 10.1523/JNEUROSCI.0028-18.2018.
Fornes, O., Castro-Mondragon, J.A., Khan, A., van der Lee, R., Zhang, X., Richmond, P.A., Modi, B.P., Correard, S., Gheorghe, M., Baranasic, D., et al. (2020). JASPAR 2020: update of the open-access database of transcription factor binding profiles. Nucleic Acids Res *48*, D87-D92. 10.1093/nar/gkz1001.
Fraser, J., Ferrai, C., Chiariello, A.M., Schueler, M., Rito, T., Laudanno, G., Barbieri, M., Moore, B.L., Kraemer, D.C., Aitken, S., et al. (2015). Hierarchical folding and reorganization of chromosomes are linked to transcriptional changes in cellular differentiation. Mol Syst Biol *11*, 852. 10.15252/msb.20156492.
Gaulton, K.J., Nammo, T., Pasquali, L., Simon, J.M., Giresi, P.G., Fogarty, M.P., Panhuis, T.M., Mieczkowski, P., Secchi, A., Bosco, D., et al. (2010). A map of open chromatin in human pancreatic islets. Nat Genet *42*, 255-259. 10.1038/ng.530.
Ghislain, J., Desmarquet-Trin-Dinh, C., Jaegle, M., Meijer, D., Charnay, P., and Frain, M. (2002). Characterisation of cis-acting sequences reveals a biphasic, axon-dependent regulation of Krox20 during Schwann cell development. Development *129*, 155-166.
Gomez-Sanchez, J.A., Carty, L., Iruarrizaga-Lejarreta, M., Palomo-Irigoyen, M., Varela-Rey, M., Griffith, M., Hantke, J., Macias-Camara, N., Azkargorta, M., Aurrekoetxea, I., et al. (2015). Schwann cell autophagy, myelinophagy, initiates myelin clearance from injured nerves. J Cell Biol *210*, 153-168. 10.1083/jcb.201503019.
Greenwald, W.W., Li, H., Benaglio, P., Jakubosky, D., Matsui, H., Schmitt, A., Selvaraj, S., D'Antonio, M., D'Antonio-Chronowska, A., Smith, E.N., and Frazer, K.A. (2019). Subtle changes in chromatin loop contact propensity are associated with differential gene regulation and expression. Nat Commun *10*, 1054. 10.1038/s41467-019-08940-5.
Hnisz, D., Abraham, B.J., Lee, T.I., Lau, A., Saint-Andre, V., Sigova, A.A., Hoke, H.A., and Young, R.A. (2013). Super-enhancers in the control of cell identity and disease. Cell *155*, 934-947. 10.1016/j.cell.2013.09.053.
Jacob, C. (2015). Transcriptional control of neural crest specification into peripheral glia. Glia *63*, 1883-1896. 10.1002/glia.22816.

Jacob, C. (2017). Chromatin-remodeling enzymes in control of Schwann cell development, maintenance and plasticity. Curr Opin Neurobiol *47*, 24-30. 10.1016/j.conb.2017.08.007.
Jessen, K.R., and Arthur-Farraj, P. (2019). Repair Schwann cell update: Adaptive reprogramming, EMT, and stemness in regenerating nerves. Glia *67*, 421-437. 10.1002/glia.23532.
Jessen, K.R., and Mirsky, R. (2008). Negative regulation of myelination: relevance for development, injury, and demyelinating disease. Glia *56*, 1552-1565. 10.1002/glia.20761.
Jessen, K.R., and Mirsky, R. (2019a). Schwann Cell Precursors; Multipotent Glial Cells in Embryonic Nerves. Front Mol Neurosci *12*, 69. 10.3389/fnmol.2019.00069.
Jessen, K.R., and Mirsky, R. (2019b). The Success and Failure of the Schwann Cell Response to Nerve Injury. Front Cell Neurosci *13*, 33. 10.3389/fncel.2019.00033.
Khalil, A.M., Guttman, M., Huarte, M., Garber, M., Raj, A., Rivea Morales, D., Thomas, K., Presser, A., Bernstein, B.E., van Oudenaarden, A., et al. (2009). Many human large intergenic noncoding RNAs associate with chromatin-modifying complexes and affect gene expression. Proc Natl Acad Sci U S A *106*, 11667-11672. 10.1073/pnas.0904715106.
Khosraviani, N., Ostrowski, L.A., and Mekhail, K. (2019). Roles for Non-coding RNAs in Spatial Genome Organization. Front Cell Dev Biol *7*, 336. 10.3389/fcell.2019.00336.
Kim, D., Paggi, J.M., Park, C., Bennett, C., and Salzberg, S.L. (2019). Graph-based genome alignment and genotyping with HISAT2 and HISAT-genotype. Nat Biotechnol *37*, 907-915. 10.1038/s41587-019-0201-4.
Kramer, N.E., Davis, E.S., Wenger, C.D., Deoudes, E.M., Parker, S.M., Love, M.I., and Phanstiel, D.H. (2022). Plotgardener: Cultivating precise multi-panel figures in R. Bioinformatics. 10.1093/bioinformatics/btac057.
Kucukural, A., Yukselen, O., Ozata, D.M., Moore, M.J., and Garber, M. (2019). DEBrowser: interactive differential expression analysis and visualization tool for count data. BMC Genomics *20*, 6. 10.1186/s12864-018-5362-x.
Kuhlbrodt, K., Herbarth, B., Sock, E., Hermans-Borgmeyer, I., and Wegner, M. (1998). Sox10, a novel transcriptional modulator in glial cells. J Neurosci *18*, 237-250.
Kuleshov, M.V., Jones, M.R., Rouillard, A.D., Fernandez, N.F., Duan, Q., Wang, Z., Koplev, S., Jenkins, S.L., Jagodnik, K.M., Lachmann, A., et al. (2016). Enrichr: a comprehensive gene set enrichment analysis web server 2016 update. Nucleic Acids Res *44*, W90-97. 10.1093/nar/gkw377.
Langmead, B., and Salzberg, S.L. (2012). Fast gapped-read alignment with Bowtie 2. Nat Methods *9*, 357-359. 10.1038/nmeth.1923.
Lee, B.T., Barber, G.P., Benet-Pages, A., Casper, J., Clawson, H., Diekhans, M., Fischer, C., Gonzalez, J.N., Hinrichs, A.S., Lee, C.M., et al. (2022). The UCSC Genome Browser database: 2022 update. Nucleic Acids Res *50*, D1115-D1122. 10.1093/nar/gkab959.
Liao, Y., Smyth, G.K., and Shi, W. (2014). featureCounts: an efficient general purpose program for assigning sequence reads to genomic features. Bioinformatics *30*, 923-930. 10.1093/bioinformatics/btt656.
Liao, Y., Smyth, G.K., and Shi, W. (2019). The R package Rsubread is easier, faster, cheaper and better for alignment and quantification of RNA sequencing reads. Nucleic Acids Res *47*, e47. 10.1093/nar/gkz114.
Love, M.I., Huber, W., and Anders, S. (2014). Moderated estimation of fold change and dispersion for RNA-seq data with DESeq2. Genome Biol *15*, 550. 10.1186/s13059-014-0550-8.

Madani Tonekaboni, S.A., Mazrooei, P., Kofia, V., Haibe-Kains, B., and Lupien, M. (2019). Identifying clusters of cis-regulatory elements underpinning TAD structures and lineage-specific regulatory networks. Genome Res *29*, 1733-1743. 10.1101/gr.248658.119.
Martinez-Moreno, M., O'Shea, T.M., Zepecki, J.P., Olaru, A., Ness, J.K., Langer, R., and Tapinos, N. (2017). Regulation of Peripheral Myelination through Transcriptional Buffering of Egr2 by an Antisense Long Non-coding RNA. Cell Rep *20*, 1950-1963. 10.1016/j.celrep.2017.07.068.
Mortazavi, A., Williams, B.A., McCue, K., Schaeffer, L., and Wold, B. (2008). Mapping and quantifying mammalian transcriptomes by RNA-Seq. Nat Methods *5*, 621-628. 10.1038/nmeth.1226.
Nora, E.P., Lajoie, B.R., Schulz, E.G., Giorgetti, L., Okamoto, I., Servant, N., Piolot, T., van Berkum, N.L., Meisig, J., Sedat, J., et al. (2012). Spatial partitioning of the regulatory landscape of the X-inactivation centre. Nature *485*, 381-385. 10.1038/nature11049.
Ong, C.T., and Corces, V.G. (2014). CTCF: an architectural protein bridging genome topology and function. Nat Rev Genet *15*, 234-246. 10.1038/nrg3663.
Oudelaar, A.M., Davies, J.O.J., Hanssen, L.L.P., Telenius, J.M., Schwessinger, R., Liu, Y., Brown, J.M., Downes, D.J., Chiariello, A.M., Bianco, S., et al. (2018). Single-allele chromatin interactions identify regulatory hubs in dynamic compartmentalized domains. Nat Genet *50*, 1744-1751. 10.1038/s41588-018-0253-2.
Palazzo, A.F., and Lee, E.S. (2015). Non-coding RNA: what is functional and what is junk? Front Genet *6*, 2. 10.3389/fgene.2015.00002.
Phanstiel, D.H., Van Bortle, K., Spacek, D., Hess, G.T., Shamim, M.S., Machol, I., Love, M.I., Aiden, E.L., Bassik, M.C., and Snyder, M.P. (2017). Static and Dynamic DNA Loops form AP-1-Bound Activation Hubs during Macrophage Development. Mol Cell *67*, 1037-1048 e1036. 10.1016/j.molcel.2017.08.006.
Picard Toolkit. (2019). https://broadinstitute.github.io/picard/.
Quinlan, A.R., and Hall, I.M. (2010). BEDTools: a flexible suite of utilities for comparing genomic features. Bioinformatics *26*, 841-842. 10.1093/bioinformatics/btq033.
Rao, S.S., Huntley, M.H., Durand, N.C., Stamenova, E.K., Bochkov, I.D., Robinson, J.T., Sanborn, A.L., Machol, I., Omer, A.D., Lander, E.S., and Aiden, E.L. (2014). A 3D map of the human genome at kilobase resolution reveals principles of chromatin looping. Cell *159*, 1665-1680. 10.1016/j.cell.2014.11.021.
Rinn, J.L., and Chang, H.Y. (2012). Genome regulation by long noncoding RNAs. Annu Rev Biochem *81*, 145-166. 10.1146/annurev-biochem-051410-092902.
Ritchie, M.E., Phipson, B., Wu, D., Hu, Y., Law, C.W., Shi, W., and Smyth, G.K. (2015). limma powers differential expression analyses for RNA-sequencing and microarray studies. Nucleic Acids Res *43*, e47. 10.1093/nar/gkv007.
Ross-Innes, C.S., Stark, R., Teschendorff, A.E., Holmes, K.A., Ali, H.R., Dunning, M.J., Brown, G.D., Gojis, O., Ellis, I.O., Green, A.R., et al. (2012). Differential oestrogen receptor binding is associated with clinical outcome in breast cancer. Nature *481*, 389-393. 10.1038/nature10730.
Sahin, M., Wong, W., Zhan, Y., Van Deynze, K., Koche, R., and Leslie, C.S. (2021). HiC-DC+ enables systematic 3D interaction calls and differential analysis for Hi-C and HiChIP. Nat Commun *12*, 3366. 10.1038/s41467-021-23749-x.
Schmitt, A.D., Hu, M., Jung, I., Xu, Z., Qiu, Y., Tan, C.L., Li, Y., Lin, S., Lin, Y., Barr, C.L., and Ren, B. (2016). A Compendium of Chromatin Contact Maps Reveals Spatially Active Regions in the Human Genome. Cell Rep *17*, 2042-2059. 10.1016/j.celrep.2016.10.061.

Sock, E., and Wegner, M. (2019). Transcriptional control of myelination and remyelination. Glia *67*, 2153-2165. 10.1002/glia.23636.
Song, L., Zhang, Z., Grasfeder, L.L., Boyle, A.P., Giresi, P.G., Lee, B.K., Sheffield, N.C., Graf, S., Huss, M., Keefe, D., et al. (2011). Open chromatin defined by DNaseI and FAIRE identifies regulatory elements that shape cell-type identity. Genome Res *21*, 1757-1767. 10.1101/gr.121541.111.
Stierli, S., Imperatore, V., and Lloyd, A.C. (2019). Schwann cell plasticity-roles in tissue homeostasis, regeneration, and disease. Glia *67*, 2203-2215. 10.1002/glia.23643.
Svaren, J., and Meijer, D. (2008). The molecular machinery of myelin gene transcription in Schwann cells. Glia *56*, 1541-1551. 10.1002/glia.20767.
Team, B.C., and Maintainer, B.P. (2019). TxDb.Rnorvegicus.UCSC.rn6.refGene: Annotation package for TxDb object(s). R package version 3.4.6.
Team, T.B.D. (2019). BSgenome.Rnorvegicus.UCSC.rn6: Full genome sequences for Rattus norvegicus (UCSC version rn6). R package version 1.4.1.
Topilko, P., Schneider-Maunoury, S., Levi, G., Baron-Van Evercooren, A., Chennoufi, A.B., Seitanidou, T., Babinet, C., and Charnay, P. (1994). Krox-20 controls myelination in the peripheral nervous system. Nature *371*, 796-799. 10.1038/371796a0.
Tripodi, I.J., Allen, M.A., and Dowell, R.D. (2018). Detecting Differential Transcription Factor Activity from ATAC-Seq Data. Molecules *23*. 10.3390/molecules23051136.
Tsai, M.C., Manor, O., Wan, Y., Mosammaparast, N., Wang, J.K., Lan, F., Shi, Y., Segal, E., and Chang, H.Y. (2010). Long noncoding RNA as modular scaffold of histone modification complexes. Science *329*, 689-693. 10.1126/science.1192002.
Weider, M., and Wegner, M. (2017). SoxE factors: Transcriptional regulators of neural differentiation and nervous system development. Semin Cell Dev Biol *63*, 35-42. 10.1016/j.semcdb.2016.08.013.
Woodhoo, A., Alonso, M.B., Droggiti, A., Turmaine, M., D'Antonio, M., Parkinson, D.B., Wilton, D.K., Al-Shawi, R., Simons, P., Shen, J., et al. (2009). Notch controls embryonic Schwann cell differentiation, postnatal myelination and adult plasticity. Nat Neurosci *12*, 839-847. 10.1038/nn.2323.
Yu, G., Wang, L.G., and He, Q.Y. (2015). ChIPseeker: an R/Bioconductor package for ChIP peak annotation, comparison and visualization. Bioinformatics *31*, 2382-2383. 10.1093/bioinformatics/btv145.
Zhang, S.J., Wu, W.L., Yang, K.Y., Chen, Y.Z., and Liu, H.C. (2017). Phenotypic changes of Schwann cells on the proximal stump of injured peripheral nerve during repair using small gap conduit tube. Neural Regen Res *12*, 1538-1543. 10.4103/1673-5374.215266.
Zhang, Y., Liu, T., Meyer, C.A., Eeckhoute, J., Johnson, D.S., Bernstein, B.E., Nusbaum, C., Myers, R.M., Brown, M., Li, W., and Liu, X.S. (2008). Model-based analysis of ChIP-Seq (MACS). Genome Biol *9*, R137. 10.1186/gb-2008-9-9-r137.